Metabolic bi-stability and hysteresis in a model microbiome community

Thesis by
Tahmineh Khazaei

In Partial Fulfillment of the Requirements for
the degree of
Doctor of Philosophy

CALIFORNIA INSTITUTE OF TECHNOLOGY
Pasadena, California

2019
(Defended May 6, 2019)

Tahmineh Khazaei
ORCID: 0000-0002-4743-2383

ACKNOWLEDGEMENTS

I would like to first express my deepest gratitude to my parents. They have made countless sacrifices for me growing up so I could have a brighter future. Throughout my graduate career, although far away, they have been here for me every single day with endless support and love. I would also like to thank my two brothers, Hamid and Arash, for always believing in me, and continuously cheering me on throughout my PhD journey.

I wish to express my sincere gratitude to my advisor, Professor Rustem Ismagilov, for his continuous support of my PhD study and for helping me grow as a research scientist. One thing that will always stick with me is his emphasis that when doing research, the bottleneck should not be resources, but science itself. And indeed, Rustem provided us with ample resources, from funding to opportunities to work with and learn from collaborators. I am very grateful for his encouragement of multi-disciplinary research, which expanded my skill sets and allowed me to work with collaborators in many different fields. I am also thankful to Rustem for giving me opportunities to learn and practice skills important for a career as a research scientist, such as writing grant applications and patent disclosures. Finally, I would like to thank Rustem for being very supportive of my exploration of career interests—I had the opportunity to spend a summer interning at Verily to learn about a career in the biotech industry, which was an invaluable experience.

I would also like to extend my warmest thanks to my committee members: Dr. Christopher Henry, Professor John Doyle, Professor Jared Leadbetter, and Professor Richard Murray. I started working with Chris a year before I joined Caltech, and since then he has kindly been continuously supportive of me. I have learned so much from him about the field of metabolic modeling, which has shaped a major portion of my thesis project. I am especially thankful to Chris for spending the time to look into and help improve my codes and mathematical models. I am very grateful for meeting John during my PhD. He has been extremely encouraging of my project and made me feel welcome as part of his own group. He has really helped me recognize and articulate the impact of my thesis project. I am extremely grateful to Jared for teaching me a great deal about microbiology and reactor microbiology. He has

always been very welcoming on each of the many spontaneous times I dropped by his office, spending countless hours teaching me and pointing me in the right direction with my research. I would like to thank Richard for his continuous support and helpful feedback about my work and for teaching Differential Equations and Dynamical Systems, where I learned the fundamentals of dynamical systems, which became a major component of my research.

There are faculty members at Caltech and outside of Caltech who I am grateful to have met during my PhD: Professor Matt Thompson and Professor Lior Pachter, for helping me to interpret data related to my research; Professor Diane Newman, for helpful discussions about my research as well as general life and career advice; Dr. Vanessa Ridaura, for always making me laugh and being an amazing mentor to work for while I interned at Verily; Professor Elaine Hsaio, an inspiring former postdoc in our lab, for her helpful feedback on my manuscript and for generously spending time with me for career advice; Professor Joseph Parker, for insightful discussions about my research and for teaching me about the potential implications in evolutionary ecology.

I would like to thank all members of the Ismagilov Lab. I had the opportunity to collaborate with and learn from many of them: Jacob Barlow and Nathan Schoepp, who I had the pleasure of working with and publishing an article together. On a separate project, I had the pleasure of working with Rory Williams, Said Bogatyrev, and Roberta Poceviciute, who are not only fantastic colleagues but have also become my good friends. I have also enjoyed collaborating with and learning from Dmitriy Zhukov and Jenia Khorosheva. I would like to extend a big thank you to Tasha Shelby, for being extremely supportive and very enjoyable to collaborate with on projects. She has been essential to the writing process in translating and articulating research projects into articles.

Finally, I am extremely grateful to my friends who truly deserve a big recognition for making these years enjoyable. Thank you for being there for me during the challenges and for celebrating the steps of accomplishment along the way.

ABSTRACT

For the past century, the mechanism for many infectious diseases has been linked to a single pathogen (per Koch's postulates); however, with the recent expanding characterization of the microbiome, it is now known that changes in the abundance and composition of species in the human microbiome, and the persistence of these altered microbiome states, can also be associated with disease. There is therefore a critical need to expand our understanding of the mechanisms that cause a stable healthy microbiome to shift into an alternate, stable disease state. Some of these microbiome disease states even paradoxically persist in seemingly unfavorable conditions, e.g., the proliferation of oxygen-sensitive microbes (anaerobes) in oxygen-exposed environments as seen in wound infections, periodontal disease and small intestinal bacterial overgrowth. In Chapter I, we use a combination of genome-scale modeling, reactor microbiology, transcriptomics, and control theory to reveal a potential mechanism for shifts and persistence of microbiome states: multi-stability and hysteresis (MSH). In our results, MSH explains how short-term, reversible changes in oxygen and carbohydrate nutrient levels lead to the persistent, essentially irreversible overgrowth of oxygen-sensitive microbiota. We find that MSH extends beyond the population level and is observed at the level of metabolism, suggesting that MSH is a general mechanism that can describe aerobe–anaerobe states in the microbiome.

Chapter II details a method for rapidly detecting the susceptibility and resistance of *Neisseria gonorrhoeae* to the antibiotic ciprofloxacin. Antimicrobial-resistant *Neisseria gonorrhoeae* is an urgent public-health threat, with continued worldwide incidents of infection and rising resistance to antimicrobials. Traditional culture-based methods for antibiotic susceptibility testing are unacceptably slow (1–2 days), resulting in the use of broad-spectrum antibiotics and the further development and spread of resistance. Critically needed is a rapid antibiotic susceptibility test (AST) that can guide treatment at the point-of-care. In our approach, we explore the use of RNA signatures, which are among the first cellular responses to drug exposure, as an indicator of antibiotic susceptibility. Using RNA sequencing, we identified antibiotic-responsive transcripts. Significant shifts (>4-fold

change) in transcript levels occurred within 5 minutes of antibiotic exposure. We designed assays for responsive transcripts with the highest abundances and fold changes, and validated gene expression using digital PCR. Using the top two markers (*porB* and *rpmB*), we correctly determined the antibiotic susceptibility and resistance of 49 clinical isolates after 10-min exposure to ciprofloxacin. RNA signatures are therefore promising as an approach on which to build rapid AST devices for *N. gonorrhoeae* at the point-of-care, which is critical for disease management, surveillance, and antibiotic stewardship efforts.

PUBLISHED CONTENT AND CONTRIBUTIONS

Chapter I: Tahmineh Khazaei, Rory L. Williams, Said R. Bogatyrev, John C. Doyle, Christopher S. Henry, Rustem F. Ismagilov. "Metabolic bi-stability and hysteresis in a model microbiome community" Submitted (2019).

Author contributions:

Tahmineh Khazaei: Hypothesis ideation with SRB. Design of study. Performed preliminary experiments with SRB: evaluating *Kp-Bt* community growth under various glucose conditions in batch culture. Built the mathematical model used in this study (Figure 1). Using the mathematical models predicted state-switching and hysteresis within the community and identified regions of bi-stability with respect to glucose and oxygen input conditions (Figure 2). Designed CSTR experiments. These experiments were performed by RLW with help from TK. Established the protocol for short chain fatty acids measurements (further optimized by RLW). Established the protocol for RNA extraction of CSTR samples for RNA sequencing. Performed the RNA extraction of all CSTR samples for RNA sequencing. Established the bioinformatics pipeline for processing and analyzing the CSTR samples (mixed-species samples). Processed and analyzed the RNA sequencing data (Figure 4). Wrote and made figures for the manuscript.

Rory L. Williams: Performed preliminary plate reader experiments testing state switching with BT/KP and BT/E. coli that determined we would use KP in CSTR experiments. Established the CSTR workflow, optimized media conditions, and performed the CSTR experiments with help from TK (Figure 2). Designed CSTR experiments with TK. Worked with Nathan Dalleska to optimize HPLC for the measurement of SCFAs in CSTR samples. Performed qPCR of all the CSTR samples (Figure 2). Characterized some of the Michaelis Menton constants used in the mathematical models. This was done

through batch experiments for growth of Bt and Kp on various substrates and Bayesian parameter inference. Helped TK in preparing the manuscript.

Said Bogatyrev: Hypothesis ideation with TK. Designed and performed preliminary experiments with TK: evaluating *Kp-Bt* community growth in batch culture as a function of substrate concentration, selectivity, and redox potential in the system.

Roberta Poceviciute: Performed HCR-FISH and DAPI staining on the bioreactor samples embedded into acrylamide gels and imaged. Created imaging figure.

Chapter II: Tahmineh Khazaei, Jacob T. Barlow, Nathan G. Schoepp, and Rustem F. Ismagilov. "RNA markers enable phenotypic test of antibiotic susceptibility in Neisseria gonorrhoeae after 10 minutes of ciprofloxacin exposure." *Scientific reports* 8, no. 1 (2018): 11606. doi: 10.1038/s41598-018-29707-w

Author contributions

Tahmineh Khazaei: Co-designed the study with NGS. Developed the computational pipeline for processing and analyzing RNA sequencing data and for selection of RNA markers. Using this pipeline, identified porB and rpmB as the top markers for this study. Established the RNA extraction protocol for *Neisseria gonorrhoeae* samples (e.g. best kit/protocol to use). Performed RNA extraction of *Neisseria gonorrhoeae* samples from all the AST experiments in this study for RNA sequencing and performed the quality assessment of the extracted RNA. (This step was after the initial AST exposures performed by NGS or JTB.) Wrote the manuscript and generated all the final figures for publication.

Jacob T. Barlow: Worked side-by-side with TK on day-to-day experimental optimization of RNA AST pipeline on CDC strains, including choice of using 16S rRNA as a control marker. Generated glycerol stocks used for the 50 CDC strains using NGS's protocol. Set up all cultures and ran all antibiotic exposures for the 50 CDC strains using NGS's protocols. Ran all qPCR and dPCR experiments for assessing changes in RNA markers. Designed and implemented statistical thresholding method for determination of differential genes. Used thresholding method to choose 4 additional markers tested. Designed and optimized primers for the additional markers. Generated visualization strategy for plots in figures 2, 3, 4, and 5 before handing off to TK to prepare final versions for paper.

Nathan G. Schoepp: Designed "high throughput" sample handling and exposure workflow for isolates used by JTB and TK. Obtained initial set of *Neisseria*

gonorrhoeae isolates from UCLA. Established *Neisseria gonorrhoeae* culturing and quantification methods which included 1) selecting and screening medias (including the one ultimately used in AST experiments) and 2) selecting and testing primers from literature for specificity, speed, and LOD. Performed initial AST exposures using *Neisseria gonorrhoeae* isolates, which TK then extracted and sequenced. Designed primers used in final manuscript for rpmB and porB markers**.** Assisted JTB in primer design for other markers by demonstrating primer design workflow and tools. Made minor contributions to manuscript including minor edits, and providing TK with graphics used in Fig. 1.

TABLE OF CONTENTS

LIST OF ILLUSTRATIONS AND/OR TABLES

Figure *Page*

Chapter 1

Metabolic Bi-stability and Hysteresis in a Model Microbiome Community

Abstract:

Changes in the species composition of the human microbiome are associated with a broad range of diseases, but elucidating causal mechanisms has been challenging. Some microbiome disease states persist in seemingly unfavorable conditions, e.g., the proliferation of aerobe–anaerobe communities in oxygen-exposed environments in wounds or small intestinal bacterial overgrowth. Using two microbes relevant to the human microbiome, we combine genome-scale mathematical modeling, bioreactor experiments, transcriptomics, and control theory to show that multi-stability and hysteresis (MSH) is a mechanism that can describe shifts to a resilient aerobe–anaerobe community. We examine the impact of changing oxygen and nutrient regimes and identify factors, including changes in metabolism and gene expression, that lead to MSH. Where MSH explains microbiome shifts, it can profoundly improve our conceptual understanding of these paradoxically persistent disease states, and thereby facilitate effective interventions.

Introduction

Many infectious diseases can be linked to a single pathogen (Koch's postulate); however, recent evidence shows that changes in the species composition and abundance of the human microbiome can also be associated with health and disease (*1-3*). Understanding the mechanisms that cause compositional shifts in healthy microbiomes, which otherwise can be remarkably stable, is challenging due to the inherent complexity of these ecosystems. A perplexing feature of some of these disturbed ecosystems is the persistence of a new microbiome state, even in seemingly unfavorable conditions. For example, in small intestinal bacterial overgrowth (SIBO), strict anaerobes that are typically found only in the colon become prominent in the small intestine and, paradoxically, persist in this oxygenated environment. Similarly, in periodontal diseases (*4*) and in wound infections, anaerobes proliferate in oxygen-exposed environments.

One potential mechanism to explain microbiome shifts and their persistence is multi-stability (*5, 6*), the concept that several steady states can exist for an identical set of system parameters. Multi-stable systems have been described in the context of ecosystems (*7-10*), and gene-regulatory networks (*11-13*). Now, with the expanding characterization of the microbiome, there are signs that multi-stability may also exist in these communities (*14-20*). For example, compositional changes in gut microbiota are implicated in inflammatory bowel disease (*21*) and obesity (*22*). Bimodal species abundance (i.e., when a microbial species is present at either high or low levels) has been interpreted as multi-stability (*23*); however, as discussed by Gonze et al., bimodality is insufficient to prove multi-stability (*5, 24*). Some multi-stable systems can additionally exhibit hysteresis, where in response to a perturbation, a system gets "stuck" in a new steady state and the former state cannot be regained by simply reversing the perturbation (*5*). The presence of hysteresis could be hypothesized from studies of the microbiome (*25*). For example, antibiotic exposures can change the microbiome composition, and have lasting effects even after removal of the antibiotic (*26, 27*). However, it has not been rigorously tested whether multi-stability and hysteresis (MSH) can arise in a microbiome-relevant community and by what mechanism.

Here, we investigate MSH in a minimally "complex" two-species system to represent the paradoxical aerobe–anaerobe microbiome communities that persist in oxygen-exposed environments. We used two organisms prevalent in SIBO (*28*): the anaerobe *Bacteroides thetaiotaomicron* (*Bt*) that breaks down complex carbohydrates (e.g. dextran) into simple sugars and short chain fatty acids (*29*), and the facultative anaerobe (aerobe) *Klebsiella pneumoniae* (*Kp*) capable of consuming oxygen, simple sugars and short chain fatty acids (*30*).

Results and Discussions

To simulate how the interplay between environmental perturbations and inter-species metabolic interactions could lead to multi-stability, we first built a mathematical model. We used the dynamic multi-species metabolic modeling (DMMM) framework (*31*) to model a community of *Kp* and *Bt* in a continuously stirred tank reactor (CSTR) (Fig. 1.1A) with continuous input flows of dextran minimal media, glucose, and oxygen. The DMMM framework uses dynamic flux balance analysis (dFBA) (*32*), which allows us to capture temporal changes in intracellular flux rates (using the genome-scale metabolic model for each species), extracellular metabolite concentrations, and species concentrations.

Next, to computationally test whether a nutrient perturbation could lead to a change in community state, we altered glucose input concentrations (Fig. 1.2A), while keeping constant all other system parameters, including oxygen input and dextran input. The model predicted that for glucose concentrations of 0.25–3 mM in the input feed (at a constant flow rate 0.7 mL/min for all conditions), the output state consisted solely of *Kp*, which we refer to as the *Kp*-only state (Fig. 1.1B). Stoichiometrically, at these glucose concentrations oxygen was not completely consumed, thus the environment was unfavorable for *Bt* growth. However, when we increased glucose input concentration to 3.25 mM, we observed a shift to a new steady state (Fig. 1.2A). At this "tipping point," the environment became sufficiently anaerobic to support the growth of *Bt*. We refer to this second distinct steady state as the *Kp–Bt* (aerobe–anaerobe) state (Fig. 1.1C). In the *Kp–Bt* state, *Kp* uses all of the available oxygen to oxidize both glucose and the simple sugars generated from the metabolism of dextran by

Bt, resulting in anaerobic conditions. Surprisingly, this *Kp–Bt* state persisted even when we systematically reversed the input of glucose below 3.25 mM, even to 0 mM. Thus, this system shows hysteresis and bi-stability: under identical input conditions of glucose and oxygen, the system can be in either of the two possible states. We then identified tipping points for population shifts in response to input oxygen variations—with glucose kept constant (Fig. 1.2B). We found that we could return the system to the *Kp*-only state by increasing oxygen levels, a state switch that was not possible by manipulating glucose concentration alone. Finally, we simulated changes in both glucose and oxygen levels and characterized the landscape of bi-stability and mono-stability in the model microbial community (Fig. 1.2C). These simulation results illustrate that even a minimal model of microbiome with co-dependence (*33*) can demonstrate dramatic MSH.

We next tested these computational predictions experimentally in a CSTR, and further explored the metabolic factors behind the dynamics of this aerobe–anaerobe community. We varied glucose concentrations and measured the steady state output composition of the microbial community by qPCR. Oxygen was introduced into the reactor by aeration at 3.4% of the gas feed (50 mL/min total gas feed) and kept constant for all conditions. For each steady-state condition, we collected three CSTR samples separated by at least one residence time.

As predicted by the mathematical models, we observed both bi-stability and hysteresis (Fig. 1.3A) experimentally. At 0.25 mM, 1 mM, and 2 mM glucose concentrations, the steady-state community consisted only of *Kp*; *Bt* was washed out under these conditions (Fig. 1.3B). The dissolved-oxygen measurements (Fig. 1.3C) confirmed that oxygen was not limiting under the selected parameter conditions, resulting in an aerobic environment unsuitable for *Bt* growth. As in the simulations, at 5 mM glucose, a new distinct steady state was reached where *Bt* grew in the presence of *Kp.* Although there was continuous oxygen flux into the reactor, the concentration of dissolved oxygen measured in the reactor was near zero. Next, to test for hysteresis, we reduced the glucose input back down to 2 mM, 1 mM, 0.25 mM, and 0 mM and found that the aerobe–anaerobe state persisted. The persistence of the *Kp–Bt*

state (instead of a return to the *Kp*-only state), confirmed hysteresis and verified that this microbial community is a bi-stable system.

The CSTR results demonstrate metabolic coupling between bacterial species with respect to carbon and oxygen. At sample point 8, there is no glucose input to the reactor, yet *Kp* continued to grow, therefore *Kp* was completely dependent on *Bt* for its carbon supply. At sample point 4, *Bt* started to grow, despite the continuous oxygen input, therefore *Bt* was dependent on removal of oxygen by *Kp*. At sample points 7 (0.25 mM glucose) and 8 (0 mM glucose), *Bt* continued to grow, despite dissolved-oxygen measurements indicating oxygen concentrations above the tolerance for *Bt* growth (Fig. 1.3C). This observation differed slightly from the model, suggesting that there may be additional biological factors beyond metabolic coupling and stoichiometric balance that can affect bi-stability. Imaging revealed that in the *Kp–Bt* state, bacterial aggregates were larger at lower glucose concentrations. Furthermore, fluorescent *in situ* hybridization (FISH) showed these aggregates contained both *Kp* and *Bt* (fig. S1.1). We hypothesize that co-aggregation provides microenvironments more favorable for *Bt* growth by further facilitating metabolic coupling between the two species, as observed in biofilms (*4*).

Gene-expression analysis of CSTR samples revealed that bi-stability also occurs at the transcriptome level in both the community and in individual species. Principal component analysis (PCA) of the community-level gene expression data showed that samples clustered based on the steady state (*Kp*-only vs. *Kp–Bt)* from which they were collected (Fig. 1.4A). Strong clustering at the community level is expected because *Bt* is absent from the *Kp*-only state. However, when we evaluated the gene-expression profile of *Kp* (Fig. 1.4B), which is present in all steady state conditions, we also found clustering based on the state of the community.

To further evaluate the proposed metabolic mechanism responsible for MSH (Fig. 1.1B,C), we compared metabolic regulation in *Kp* in the *Kp–Bt* state and the *Kp*-only state. We used a method from the Neilsen lab (*34*) to collect topological information from the genome-scale metabolic models and combine it with gene-expression data to identify reporter metabolites

that maximally differ between the two states. Among the top reporter metabolites were pyruvate, phosphoenolpyruvate, glucose, and glucose-6-phosphate (table S1.3), suggesting that the phosphotransferase system (PTS), which is involved in sugar transport, is upregulated in the *Kp*–only state relative to the *Kp-Bt* state (Fig. 1.4C–D). In the *Kp–Bt* state, genes involved in the alpha-glucoside linked substrates were upregulated (Fig. 1.4E), suggesting that *Kp* obtains some of its carbon source from oligosaccharides. These oligosaccharides are released into the environment by *Bt* through the breakdown of dextran by dextranase, an extracellular endohydrolase (*35*). *Bt* utilizes these oligosaccharides by hydrolyzing them using glucan-1,3-alpha-glucosidases. As expected, both dextranase (*dexA*) and glucan-1,3-alpha-glucosidase (*gaa*) were found to be highly expressed in *Bt* in the *Kp–Bt* state (Fig. 1.4E).

Our analysis (Fig. 1.4F) also suggested an upregulation of acetate utilization by *Kp* in the *Kp–Bt* state as inferred from the upregulation of acetate permease and acetyl-coenzyme A synthetase. Additionally, *Kp* genes involved in lactate utilization were upregulated in the *Kp–Bt* state. Upon oxygen exposure, *Bt* is known to produce lactate (*36*). Bi-stability of gene expression extended to the anaerobic metabolic pathway for propanediol utilization (Fig. 1.4G), which results in formation of metabolic micro-compartments (*37*). We thus infer that a subpopulation of *Kp* was undergoing anaerobic metabolism in samples 4 and 5 (of the *Kp–Bt* state), where the dissolved oxygen concentrations in the reactor were lowest (Fig. 1.3C). Overall, these results were consistent with the basic mechanism for MSH (Figure 1B–C) and reveal that MSH extends to the expression of genes and pathways involved in metabolic coupling between the species.

In this work, we used genome-scale mathematical modeling, bioreactor experiments, transcriptomics, and control theory in a model microbiome to show that MSH is a mechanism that can describe shifts and persistence of a model microbiome aerobe–anaerobe community under seemingly paradoxical conditions (e.g., oxygen-exposed environments). Identifying and interpreting MSH in human microbiomes and microbiome-associated diseases would require carefully designed longitudinal measurements and

models that take into account the full complexity of microbiomes, their spatial structure, and host responses. If MSH is found, it would have profound conceptual impact. To understand and control microbial communities without MSH, one currently relies on a well-established conceptual connection between correlation, causation, and control. Consider points S1-S3 (Fig. 1.3). The levels of *Kp* correlate with the input glucose concentration—from a known input glucose concentration, one can infer a steady-state *Kp* concentration and vice versa. Input glucose concentration is the causal factor and therefore it can be used to control the steady-state levels of *Kp*. If MSH is identified in microbiomes, it would break this familiar conceptual connection between causation and correlation. Consider the region of hysteresis (points S1-S3 and S5-S7, Fig. 1.3). The observed steady-state levels of *Kp* no longer correlate with the input glucose concentration. At 2 mM input glucose, the system could be in either the *Kp*-only state S3 or the *Kp–Bt* state S5. At ~650x10^6 CFU/mL of *Kp*, the input glucose levels could be either 0.25 mM or 2 mM. Although there is no correlation, input glucose concentration remains the causal factor. Furthermore, under MSH, establishing causation is insufficient for achieving control: although input glucose concentration is the causal factor responsible for changes in the community state, it cannot be used to fully control the community (i.e. one cannot use changes in glucose inputs to revert the *Kp–Bt* state back to the *Kp*-only state). Alternative control strategies (e.g. changes in oxygen levels or disruption of metabolic coupling), derived from appropriate models, would need to be deployed under MSH. Therefore, recognizing whether and when MSH exists in human microbiomes and human diseases will be critical for interpreting correlation and causation, and for designing therapeutic control strategies that can steer microbial communities to desirable states.

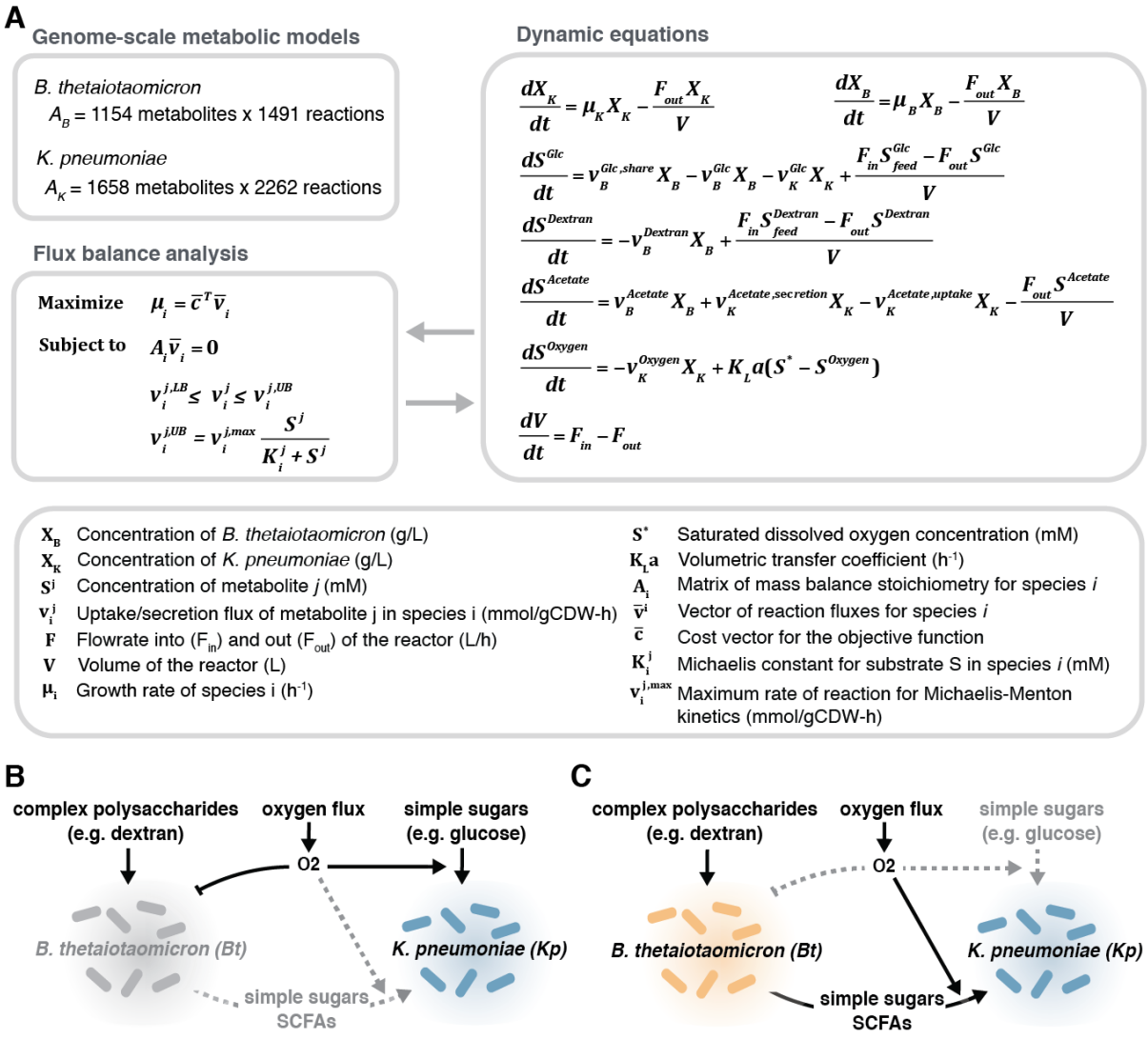

Fig. 1.1 A multi-stable model system consisting of *Klebsiella pneumoniae (Kp)*, a facultative anaerobe, and *Bacteroides thetaiotaomicron (Bt)*, an anaerobe, that is relevant to the human gut microbiome. (**A**) Dynamic equations describing the model system can be solved with dynamic flux-balance analysis utilizing each species' genome-scale metabolic model. (**B**) In the *Kp*-only state, *Bt* does not grow and *Kp* utilizes external sugars and short chain fatty acids. (**C**) In the *Kp–Bt* state, *Bt* can grow and break down complex polysaccharides into simple sugars and short chain fatty acids, which *Kp* can utilize to maintain reduced oxygen levels favorable for *Bt* growth.

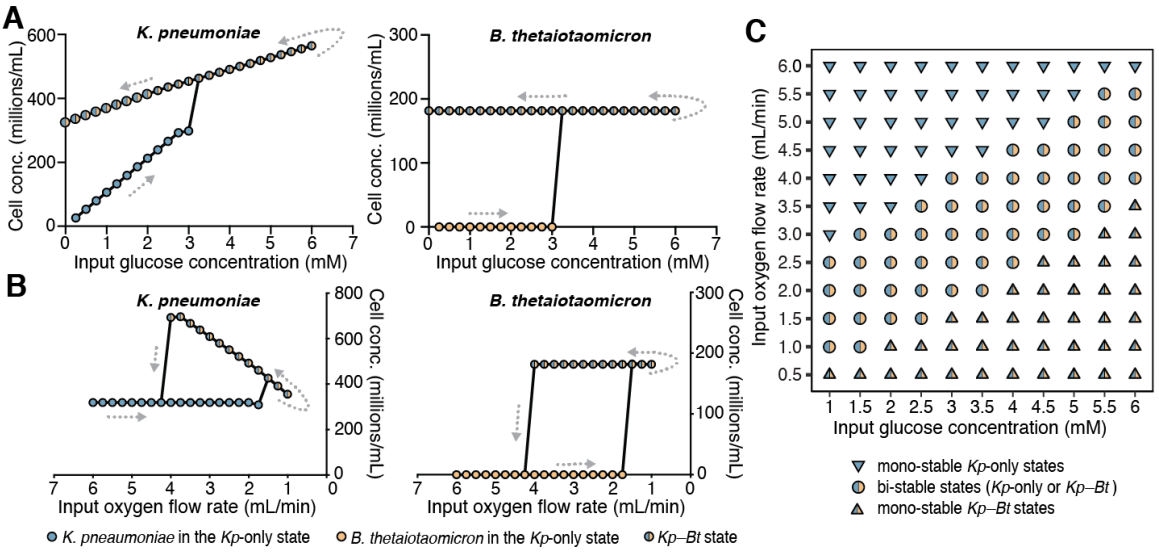

Fig. 1.2. Simulations illustrating bi-stability and hysteresis in the microbial community with respect to environmental perturbations. Cell concentrations as a factor of (**A**) glucose-concentration variations in the input feed under constant input oxygen flow rate, and (**B**) input oxygen flow variations under constant glucose concentrations in the input feed. Each point represents the steady-state concentration for the given species in the community after a 50-h simulation. (**C**) Regions of stability as a function of glucose concentrations in the input feed and oxygen flow rates into the reactor. In regions of bi-stability (circles), the community can exist in either a *Kp*-only state or a *Kp–Bt* (aerobe–anaerobe) state under the same conditions. In regions of mono-stability (triangles), the community can only exist in either a *Kp*-only or a *Kp–Bt* state.

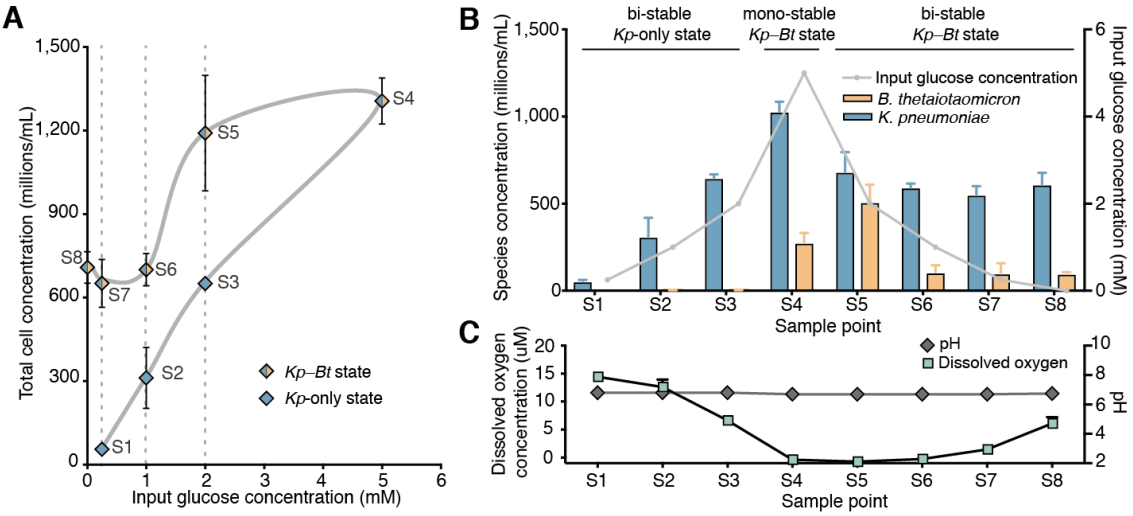

Fig. 1.3. Bi-stability and hysteresis of *K. pneumoniae* (*Kp*) and *B. thetaiotaomicron* (*Bt*) community in a CSTR. (**A**) Total cell concentrations collected at the eight different steady state sample points (S1–S8) from the CSTR measured by qPCR. (**B**) Cell concentrations for each individual species in the community measured by qPCR. (**C**) pH and dissolved-oxygen concentrations measured in the CSTR for each sample point. Error bars are S.D. of three replicates collected (separated by >1 residence time) from the CSTR for each of the eight steady-state glucose conditions.

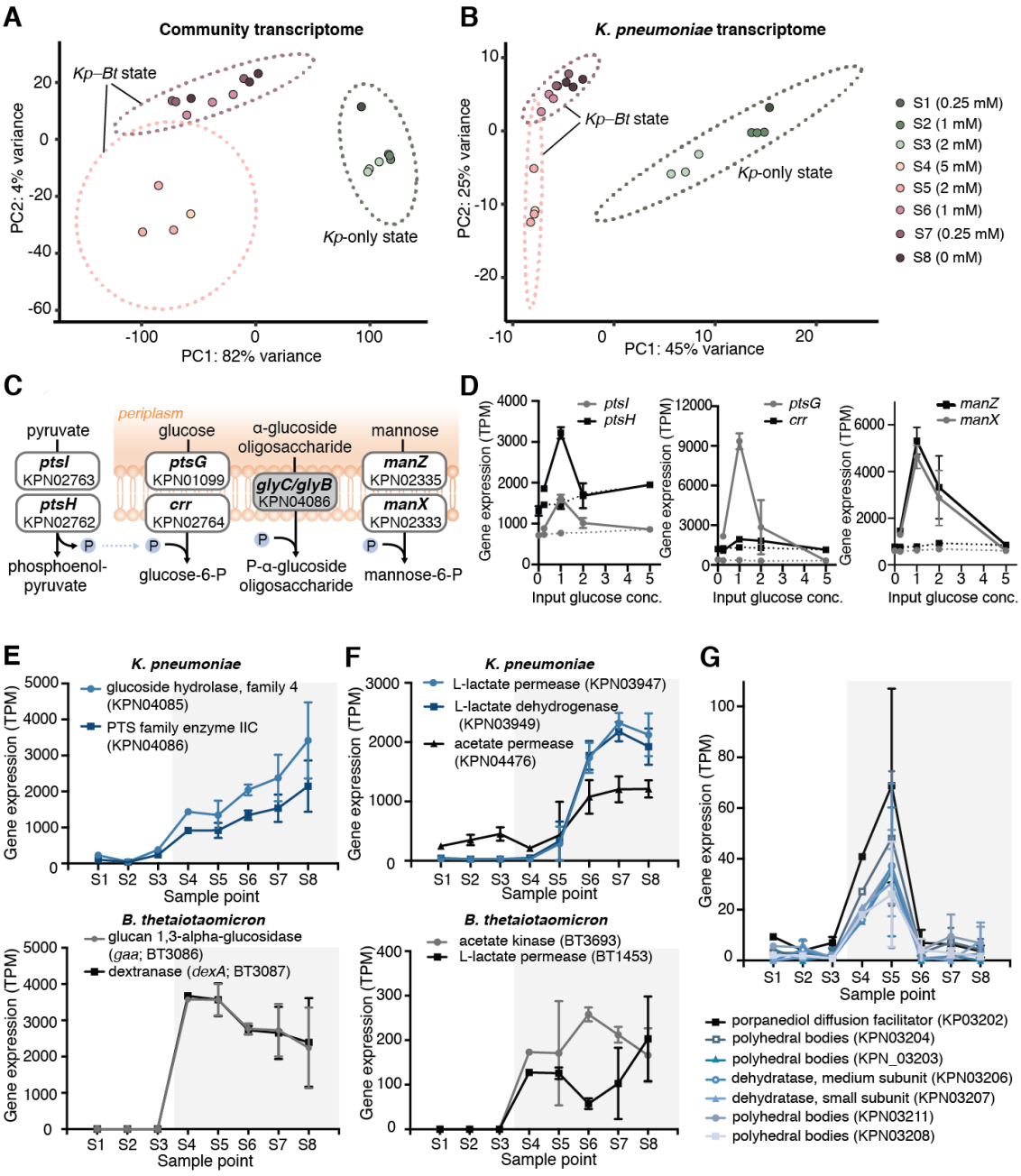

Fig. 1.4. Gene-expression analysis of CSTR steady-state samples. (**A**) PCA of the community transcriptome; each dot represents the combined transcriptome of *K. pneumoniae* (*Kp*) and *B. thetaiotaomicron* (*Bt*) for each sample (S1-S8). (**B**) PCA of the *Kp* transcriptome. (**C**) The most differentially regulated pathway between the *Kp*-only and the *Kp–Bt* states is the phosphotransferase system (PTS); the grey box indicates the upregulated gene; white

boxes are downregulated. (**D**) PTS genes downregulated in the *Kp–Bt* state. Solid lines represent the *Kp*-only state and dashed lines represent the *Kp–Bt* state. (**E**) Gene expression, in transcripts per million (TPM), of oligosaccharide uptake in *Kp* and dextran metabolism to oligosaccharides in *Bt* for each steady-state sample point. (**F**) Expression of genes involved in acetate and lactate utilization in *Kp,* and acetate and lactate production in *Bt* for each CSTR sample. (**G**) Expression of the propanediol-utilization pathway in *Kp.* (**E–G**) Unshaded regions are the *Kp*-only state; the gray shaded region is the *Kp–Bt* state.

References:

1. V. Singh, S. Proctor, B. Willing, Koch's postulates, microbial dysbiosis and inflammatory bowel disease. *Clin. Microbiol. and Infect.* **22**, 594-599 (2016).
2. L. Zhao, The gut microbiota and obesity: from correlation to causality. *Nat. Rev. Microbiol.* **11**, 639 (2013).
3. R. Blumberg, F. Powrie, Microbiota, disease, and back to health: a metastable journey. *Sci. Transl. Med.* **4**, 137rv137 (2012).
4. D. Bradshaw, P. Marsh, G. Watson, C. Allison, Oral anaerobes cannot survive oxygen stress without interacting with faculItative/aerobic species as a microbial commmunity. *Lett. Appl. Microbiol.* **25**, 385-387 (1997).
5. D. Gonze, L. Lahti, J. Raes, K. Faust, Multi-stability and the origin of microbial community types. *ISME J.* **11**, 2159 (2017).
6. S. A. Shetty, F. Hugenholtz, L. Lahti, H. Smidt, W. M. de Vos, Intestinal microbiome landscaping: insight in community assemblage and implications for microbial modulation strategies. *FEMS Microbiol. Rev.* **41**, 182-199 (2017).
7. J. H. Connell, W. P. Sousa, On the evidence needed to judge ecological stability or persistence. *Am. Nat.* **121**, 789-824 (1983).
8. M. Hirota, M. Holmgren, E. H. Van Nes, M. Scheffer, Global resilience of tropical forest and savanna to critical transitions. *Science* **334**, 232-235 (2011).
9. A. Schröder, L. Persson, A. M. De Roos, Direct experimental evidence for alternative stable states: a review. *Oikos* **110**, 3-19 (2005).
10. T. Bush *et al.*, Oxic-anoxic regime shifts mediated by feedbacks between biogeochemical processes and microbial community dynamics. *Nat. Commun.* **8**, 789 (2017).
11. O. S. Venturelli, H. El-Samad, R. M. Murray, Synergistic dual positive feedback loops established by molecular sequestration generate robust bimodal response. *Proc. Natl. Acad. Sci. U.S.A.* **109**, E3324-E3333 (2012).
12. D. Dubnau, R. Losick, Bistability in bacteria. *Mol. Microbiol.* **61**, 564-572 (2006).

13. J. E. Ferrell Jr, Self-perpetuating states in signal transduction: positive feedback, double-negative feedback and bistability. *Curr. Opin. Cell Biol.* **14**, 140-148 (2002).
14. G. D. Wu *et al.*, Linking long-term dietary patterns with gut microbial enterotypes. *Science* **334**, 105-108 (2011).
15. F. Hildebrand *et al.*, Inflammation-associated enterotypes, host genotype, cage and inter-individual effects drive gut microbiota variation in common laboratory mice. *Genome Biol.* **14**, R4 (2013).
16. Y. Zhou *et al.*, Exploration of bacterial community classes in major human habitats. *Genome Biol.* **15**, R66 (2014).
17. T. Ding, P. D. Schloss, Dynamics and associations of microbial community types across the human body. *Nature* **509**, 357 (2014).
18. J. Ravel *et al.*, Vaginal microbiome of reproductive-age women. *Proc. Natl. Acad. Sci. U.S.A.* **108**, 4680-4687 (2011).
19. M. Arumugam *et al.*, Enterotypes of the human gut microbiome. *Nature* **473**, 174 (2011).
20. G. Falony *et al.*, Population-level analysis of gut microbiome variation. *Science* **352**, 560-564 (2016).
21. D. Gevers *et al.*, The treatment-naive microbiome in new-onset Crohn's disease. *Cell Host Microbe.* **15**, 382-392 (2014).
22. I. Cho, M. J. Blaser, The human microbiome: at the interface of health and disease. *Nat. Rev. Genet.* **13**, 260 (2012).
23. L. Lahti, J. Salojärvi, A. Salonen, M. Scheffer, W. M. De Vos, Tipping elements in the human intestinal ecosystem. *Nature Commun.* **5**, 4344 (2014).
24. M. Scheffer *et al.*, Early-warning signals for critical transitions. *Nature* **461**, 53 (2009).
25. P. Gajer *et al.*, Temporal dynamics of the human vaginal microbiota. *Sci. Transl. Med.* **4**, 132ra152-132ra152 (2012).

26. L. Dethlefsen, D. A. Relman, Incomplete recovery and individualized responses of the human distal gut microbiota to repeated antibiotic perturbation. *Proc. Natl. Acad. Sci. U.S.A.* **108**, 4554-4561 (2011).
27. C. Jernberg, S. Löfmark, C. Edlund, J. K. Jansson, Long-term ecological impacts of antibiotic administration on the human intestinal microbiota. *ISME J.* **1**, 56 (2007).
28. Y. Bouhnik *et al.*, Bacterial populations contaminating the upper gut in patients with small intestinal bacterial overgrowth syndrome. *Am. J. Gastroenterol.* **94**, 1327-1331 (1999).
29. A. Heinken, S. Sahoo, R. M. Fleming, I. Thiele, Systems-level characterization of a host-microbe metabolic symbiosis in the mammalian gut. *Gut Microbes.* **4**, 28-40 (2013).
30. Y. C. Liao *et al.*, An experimentally validated genome-scale metabolic reconstruction of Klebsiella pneumoniae MGH 78578, iYL1228. *J. Bacteriol.* **193**, (2011).
31. K. Zhuang *et al.*, Genome-scale dynamic modeling of the competition between Rhodoferax and Geobacter in anoxic subsurface environments. *ISME J.* **5**, 305 (2011).
32. R. Mahadevan, J. S. Edwards, F. J. Doyle III, Dynamic flux balance analysis of diauxic growth in Escherichia coli. *Biophys. J.* **83**, 1331-1340 (2002).
33. O. S. Venturelli *et al.*, Deciphering microbial interactions in synthetic human gut microbiome communities. *Mol. Syst. Biol.* **14**, e8157 (2018).
34. K. R. Patil, J. Nielsen, Uncovering transcriptional regulation of metabolism by using metabolic network topology. *Proc. Natl. Acad. Sci. U.S.A.* **102**, 2685-2689 (2005).
35. D. A. Ravcheev, A. Godzik, A. L. Osterman, D. A. Rodionov, Polysaccharides utilization in human gut bacterium Bacteroides thetaiotaomicron: comparative genomics reconstruction of metabolic and regulatory networks. *BMC Genomics.* **14**, 873 (2013).

36. S. Mishra, J. A. Imlay, An anaerobic bacterium, Bacteroides thetaiotaomicron, uses a consortium of enzymes to scavenge hydrogen peroxide. *Mol. Microbiol.* **90**, 1356-1371 (2013).
37. E. I. Tocheva *et al.*, Structure and expression of propanediol utilization microcompartments in Acetonema longum. *J. Bacteriol.* **196**, 1651-1658 (2014).
38. J. D. Orth, I. Thiele, B. Ø. Palsson, What is flux balance analysis? *Nat. Biotechnol.* **28**, 245 (2010).
39. W. R. Harcombe *et al.*, Metabolic resource allocation in individual microbes determines ecosystem interactions and spatial dynamics. *Cell Rep.* **7**, 1104-1115 (2014).
40. G. Gosset, Improvement of Escherichia coli production strains by modification of the phosphoenolpyruvate: sugar phosphotransferase system. *Microb. Cell Fact.* **4**, 14 (2005).
41. E. Wolin, M. J. Wolin, R. Wolfe, Formation of methane by bacterial extracts. *J. Biol. Chem.* **238**, 2882-2886 (1963).

Supplementary Materials

Materials and Methods

Model development

For the computational simulations, we used the dynamic multispecies metabolic modeling (DMMM) framework (*31*), which is an extension of dynamic flux balance analysis applied to microbial communities. The system is described as a continuous stirred tank reactor (CSTR) with the following mathematical formulation:

$$\frac{dV}{dt} = F_{in} - F_{out} \quad (1)$$

$$\frac{dX_i}{dt} = \mu_i X_i - \frac{F_{out} X_i}{V} \quad (2)$$

$$\frac{dS^j}{dt} = \sum_i v_i^j X_i + \frac{F_{in} S_{feed}^j - F_{out} S^j}{V} \quad (3)$$

$$\frac{dS^{oxygen}}{dt} = \sum_i v_i^{oxygen} X_i + K_L a(S^* - S^{oxygen}) \quad (4)$$

Here, V, is the volume of the reactor, X_i is the biomass (g/L) of the ith microbial species. S^j is the concentration (mM) of the jth metabolite, F_{in} is the rate of flow (L/h) into the reactor, F_{out} is the rate of flow (L/h) out of the reactor, S_{feed}^j is the concentration of the jth metabolite in the feed stream, μ_i (h^{-1}) is the growth rate of the ith microbial species, and v_i^j is the metabolic flux of the jth substrate in the ith microbial species. The set of differential equations are solved using the following analytical approximation:

$$V_f = V_0 + (F_{in} - F_{out})\Delta T \quad (5)$$

$$X_f = X_{i,0} e^{\left(\mu_i - \frac{F_{in}}{V_0}\right)\Delta T} \quad (6)$$

$$S_f^j = S_0^j + \sum_i [v_i^j \frac{V_0}{\mu_i V_0 - F_{in}} (X_{i,0}\, e^{\left(\mu_i - \frac{F_{in}}{V_0}\right)\Delta T} - X_{i,0})] + \frac{F_{in}(S_{feed}^j - S^j)}{V_0} \Delta T \quad (7)$$

At the beginning of every time step (ΔT), the parameters μ_i and v_i^j are calculated using flux

balance analysis (FBA) from genome-scale models and fed back into equations (5) and (6). This process is repeated for all time intervals in the simulated time period. Genome-scale metabolic models are used to establish genotype-phenotype relationships and capture the metabolic capabilities of each model organism. We used the published iYL1228 model of *Klebsiella pneumoniae (Kp)* MGH 78578 (*30*) and the published iAH991 model of *Bacteroides thetaiotaomicron (Bt)* VPI 5482 *(29)*. A pathway for dextran uptake and hydrolysis to glucose was added to the iAH991 model. The pathway lumps hydrolysis of dextran to glucose into a single reaction. In this lumped reaction, we assume that 50% of the glucose produced from dextran by *Bt* can be released into the environment for shared use. For the purpose of the simulations, dextran is assumed to be 100 glucose units. The genome-scale models are solved by flux balance analysis (FBA) (*38*) at each time point:

$$\max c^T \overline{v_i} \qquad (8)$$
$$s.t.\ A_i \overline{v_i} = 0$$
$$\bar{v}_{i,lb} < \overline{v_i} < \bar{v}_{i,ub}$$

where c is the cost vector, $\bar{v}$ is the vector of fluxes, and A is the matrix of mass balance stoichiometries. The uptake fluxes are bounded by Michaelis–Menten kinetics:

$$v_{i,ub}^{j} = v_i^{j,max} \frac{S^j}{K_m + S^j} \qquad (9)$$

The values for $v_i^{j,max}$ and K_m for some of the metabolites in the model were estimated from batch experiments. Batch culture experiments were carried out in a 96-well flat-bottom plate. Overnight cultures were grown anaerobically in minimal medium. Either 0.5% w/v dextran or 0.5% w/v glucose were diluted 1:20 (for *Bt*) and 1:100 (for *Kp*), and outgrown to mid-log phase. The cultures were then pelleted and re-suspended at OD 1 (for *Bt*) and OD 0.1 (for *Kp*) in carbon-free minimal medium. We added 10 µL of cells to 200 µL of minimal medium containing various concentrations (0.125 – 0.5% w/v) of the carbon source. The plate was incubated at 37 °C and OD600 measured every 10 min. For batch cultures, Monod growth kinetics was assumed:

$$\frac{dX}{dt} = X\mu_{max}\frac{S}{S+K} \quad (10)$$

$$\frac{dS}{dt} = -v_{max}\frac{S}{S+K} \quad (11)$$

Growth data from replicate wells of multiple concentrations of carbon source were fitted simultaneously using Bayesian parameter estimation implemented with Markov chain Monte Carlo (MCMC). Individual growth curves were allowed to have distinct initial cell concentrations and background values, with other parameters held constant. The fitted parameters are presented in Table S1 and Fig S1. For all other metabolites captured in the differential equations, the K_m and v_{max} values are assumed to be the same (v_{max} of 10 mmol/gCDW·h and K_m of 0.01 mM), based on literature for *Escherichia coli (39, 40)*.

Values for parameters and initial conditions used in the model are presented in Table S2. Initial conditions are chosen to represent experimental setup, whereby we first establish a steady state for *Kp* in the CSTR before inoculating *Bt*. Therefore, in the models we start with a higher concentration of *Kp* than *Bt*. The initial conditions for *Kp* in the reactor is arbitrarily chosen to be the experimentally measured mono-culture steady concentration of *Kp* at an input glucose concentration of 0.25 mM. The initial conditions for *Bt* in the reactor is 0.0015 g/L, which is equivalent to addition of 1 mL of OD 1 *Bt* into the reactor, as done experimentally. For most steady state conditions, glucose is limiting and therefore the initial conditions for glucose concentration in the reactor is chosen to be 0mM.

To computationally identify the regions of stability with respect to glucose and oxygen (Fig. 2C and Fig. S3), we varied oxygen input flow rates at constant input glucose concentration for each glucose condition examined. We evaluated 11 glucose conditions ranging from 1 mM to 6 mM. For each given glucose input concentration, we started with oxygen at an input flow rate of 6 mL/min and ran the simulation for 50 h to ensure the system reached a steady state. We then decreased the oxygen input by 0.5 mL/min intervals down to 0.5 mL/min, for each oxygen condition, ensuring the system reached a steady state (we refer to the 6mL/min - 0.5mL/min oxygen variations for a given constant glucose input concentration as the "forward simulations"). The concentration of oxygen input at which

Bt starts to grow is identified as the "tipping point" to the mono-stable *Kp–Bt* state. After running the 0.5mL/min oxygen simulation we increased the concentration back to 6 mL/min at intervals of 0.5 mL/min (we refer to the 0.5 mL/min - 6 mL/min oxygen variations as the "reverse simulations"). The concentration of oxygen at which *Bt* can no longer grow and gets washed out is identified as "tipping point" to the mono-stable *Kp*-only state. The region between these two tipping points to the mono-stable *Kp–Bt* state in the forward simulations and the mono-stable *Kp*-only state in the reverse simulations is identified as the region of bi-stability. The colors in Fig. S3 represent the steady state concentration of *Kp* in the "reverse simulations" divided by the steady state concentration of *Kp* in the "forward simulations." In regions of mono-stability, the concentration of *Kp* is similar in both the "forward" and "reverse simulations", and therefore has a value of approximately 1.

Continuous culture of *K. pneumoniae* and *B. thetaiotaomicron*

Continuous culture experiments were carried out in a 500 mL bioreactor (Mini-bio Applikon Biotechnology, Delft, Netherlands) with a total culture volume of 200 mL. Minimal media (3.85 g/L KH_2PO_4, 12.48 g/L K_2HPO_4, 1.125 g/L $(NH_4)_2SO_4$, 1X MMS (20X MMS: 17.6 g/L NaCl, 0.4 g/L $CaCl_2$, 0.4 g/L $MgCl_2$×6H2O, 0.2 g/L $MnCl_2$×4H2O, 0.2 g/L $CoCl_2$×6H2O), 10 mL/L Wolfe's mineral solution(*41*), 10 mL/L Wolfe's vitamin solution(*41*), 4.17 µM FeSO4×7H20, 0.25 mM cysteine, 1 µM menadione, 2 µM resazurin, 1 g/L dextran (Sigma D5376, avg. mol. wt 1.5e6-2e6) and glucose at varying concentrations) was purged with 100% N_2, stored under anaerobic conditions prior to use, and maintained under N_2 during operation of CSTR. The bioreactor was aerated with 50 mL/min total gas (1.7 mL/min O_2, 5 mL/min CO_2, and balance of N_2), and agitated with two six-bladed Rushton turbines operated at 750 rpm. Temperature was maintained at 37°C, and a residence time of 5 h (40 ml/h flowrate) was used for all experiments. Dissolved oxygen, pH, and biomass were monitored throughout. For initial inoculation of *Kp*, 1 mL of OD 1 culture was injected through the septum, and grown in batch culture until stationary phase (indicated by levelling of the biomass reading and increase of dissolved oxygen levels) before beginning

continuous culture. For each steady-state condition, three samples separated by at least one residence time were collected. For introduction of *Bt*, a log phase (OD 0.6-0.8) anaerobic culture grown in minimal media with 0.5% dextran and 2mM cysteine was pelleted (5 min at 3500 g) and washed twice using dextran/glucose-free anaerobic minimal media. Cells were carbon-starved at 37 °C for 30 min, washed (once), and re-suspended in dextran/glucose-free minimal media to OD 1. We used 1 mL of this *Bt* cell suspension for inoculation into the reactor and a sample was collected immediately after inoculation. A subsequent sample was collected for quantification after at least 2 residence times had passed. In the *Kp*-only state conditions (0.25 mM, 1 mM, 2 mM glucose), *Bt* is washed out, as described in the results section. To ensure reproducibility of a washout for these conditions, the *Bt* inoculation and sample collection process was repeated a total of three times. In *Kp–Bt* state conditions (5 mM, 2 mM, 1 mM, 0.25 mM, and 0 mM glucose), where *Bt* growth persisted, re-inoculation of *Bt* was no longer necessary for each new glucose steady state condition; three samples separated by at least one residence time were collected for each steady state condition. To collect samples, ~0.5 mL of culture was removed from the bioreactor in a 3 mL luer-lock syringe and discarded before collection of 1.5–2 mL culture. Supernatant from 700 µL of the collected sample was stored at -80 °C for SCFA analysis, a 50 µL sub-sample was treated with DNAse (2.5 µL of NEB DNase I 2000 u/mL per 50 µL) for subsequent DNA extraction, and two 250 µL aliquots were used for extraction of RNA.

Quantification of bacterial abundance

Chemostat culture samples were treated with NEB DNAse I (100 u/mL final concentration) for 10 min at 37°C immediately after collection. DNA was extracted using the ZyGEM prepGEM™ Bacteria kit (ZyGEM, Southampton, England) according to the manufacturer's protocol. Samples were extracted in 100 uL total volume (20 µL culture sample and 80 µL of extraction mixture), incubated at 37 °C for 15 min, 75 °C for 5 min, 95 °C for 5 min, then cooled to 4 °C. DNA was stabilized by adding 10X TE to a final concentration of 1X TE before storage at 4 °C. Extracted DNA was quantified by qPCR using the Eco Real-time PCR system (Illumina, San Diego, CA, USA). The components in the qPCR mix used in this

study were as follows: 1 µL of extracted DNA, 1X SsoFast™ EvaGreen Supermix (Bio-Rad Laboratories, Hercules, CA, USA), 500 nM forward primer, and 500 nM reverse primer. For detection of each bacterial species in the community primer sets specific to *Bt* (forward primer: 5′-GGAGTTTTACTTTGAATGGAC-3′; reverse primer: 5′-CTGCCCTTTTACAATGGG-3') and *Kp* (forward primer: 5′-ATTTGAAGAGGTTGCAAACGAT-3′; reverse primer: 5′-TTCACTCTGAAGTTTTCTTGTGTT-3′) were used. Quantification of cell concentrations were determined using DNA standards of single species prepared using 10X serial dilutions of log phase cultures extracted as above. Cell concentrations of standards were determined by hemocytometer. For conversion of OD and cell concentration to biomass concentration (gram cell dry weight/L), 100 mL of culture for each individual species incubated anaerobically at 37 °C was harvested and pellets were dried at 80°C for ~48 h before recording mass.

RNA sequencing and analysis

From the chemostat samples, a 250 µL aliquot was used for RNA extraction. The freshly collected chemostat sample was immediately placed into Qiagen RNAprotect Bacteria Reagent (Qiagen, Hilden, Germany) for RNA stabilization. RNA was extracted using the Enzymatic Lysis of Bacteria protocol of the Qiagen RNeasy Mini Kit and processed according to the manufacturer's protocol. DNA digestion was performed during extraction using the Qiagen RNase-Free DNase Set. The quality of extracted RNA was measured using an Agilent 2200 TapeStation (Agilent, Santa Clara, CA, USA). Extracted RNA samples were prepared for sequencing using the NEBNext Ultra RNA Library Prep Kit for Illumina (New England Biolabs, Ipswitch, MA, USA) and the NEBNExt Multiplex Oligos for Illumina. Libraries were sequenced at 100 single base pair reads and a sequencing depth of 10 million reads on an Illumina HiSeq 2500 System (Illumina, San Diego, CA, USA) at the Millard and Muriel Jacobs Genetics and Genomics Laboratory, California Institute of Technology. Raw reads from the sequenced libraries were subjected to quality control to filter out low-quality reads and trim the adaptor sequences using Trimmomatic (v. 0.35). Reads that aligned to

rRNA and tRNA of *Bt* and *Kp* were first removed, as those sequences contain overlapping reads between the two species. Each sample was then separately aligned to *Bt* VPI-5482 (Genome accession number: GCA_000011065.1) and *Kp* MGH-78578 (Genome accession number: GCA_000016305.1) using Bowtie2 (v. 2.2.5) and quantified using the Subread package (v. 1.5.0-p1). Gene expression was defined in transcripts per million (TPM) for each species.

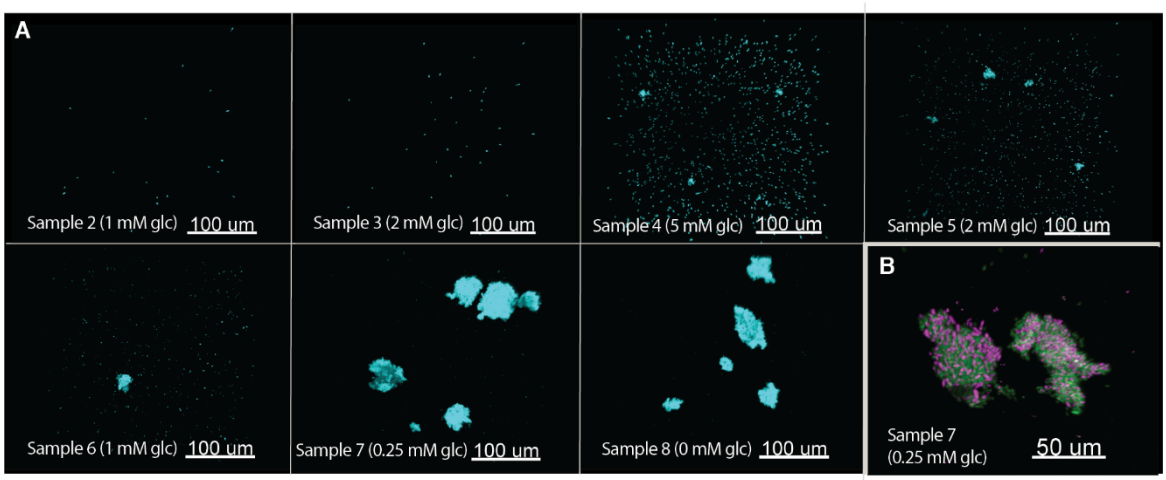

Fig. S1.1. Imaging of samples collected from the continuously stirred tank reactor experiments. (**A**) Total bacteria staining of each sample using DAPI (**B**) The species composition of aggregates using the GAM42a (green) and CFB560 probe (pink) for Gammaproteobacteria and Bacteroidetes, respectfully.

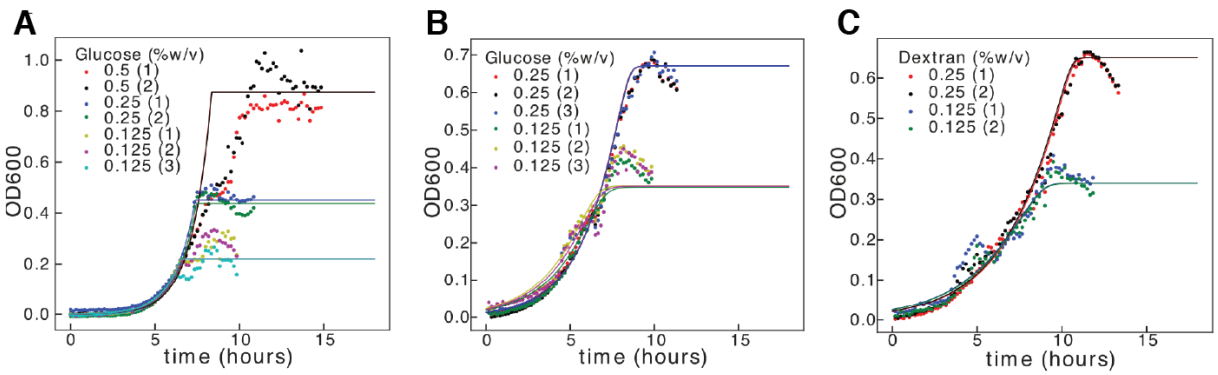

Fig. S1.2. Bayesian parameter fitting of K and v_{max} to experimental batch growth data for (**A**) *Klebsiella pneumoniae* on glucose (**B**) *Bacteroides thetaiotaomicron* on glucose, and (**C**) *Bacteroides thetaiotaomicron* on dextran. Two technical replicates were used for each concentration of substrate examined.

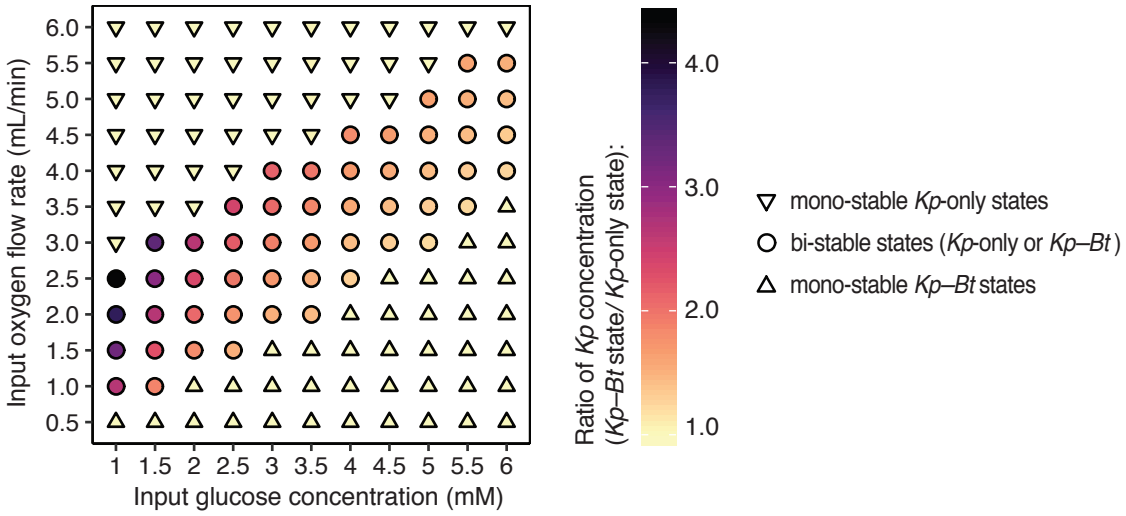

Fig. S1.3. **A quantitative view of regions of stability as a function of glucose concentrations in the input feed and oxygen flow rates into the reactor.** In regions of bi-stability (circles), the community can exist in either a *Kp*-only state or a *Kp–Bt* (aerobe–anaerobe) state under the same conditions. In regions of mono-stability (triangles), the community can only exist in either a *Kp*-only or a *Kp–Bt* state. Deviation from yellow indicates the increase of *Kp* concentration in the *Kp–Bt* state relative to the *Kp*-only state (e.g. concentration of *Kp* in *Kp–Bt* state divided by the concentration of *Kp* in the *Kp*-only state).

Table S1.1. Bayesian parameter estimation for K and v_{max} used in the Michaelis–Menten equations to constrain nutrient uptake flux rates for flux balance analysis calculations.

Species	Carbon Source	K (mM)	Vmax (mmol/gCDW·h)
K. pneumoniae	Glucose	0.00005	26.1
B. *thetaiotaomicron*	Glucose	1.4	10.9
B. *thetaiotaomicron*	Dextran	0.008	0.08

Table S1.2. Values for the parameters used in the dynamic flux balance analysis simulations.

Parameter	Value
Initial glucose concentration	0 mM
Initial dextran concentration	0.06 mM
Initial oxygen concentration	$S^* = (\frac{\text{Input O2 flowrate}}{\text{Total flowrate}})$/(O2 fraction in air) x (dissolved oxygen saturation) ▪ Input oxygen flow rate = varies ▪ Total flow rate = 50 mL/min ▪ Oxygen fraction in air = 0.2095 ▪ Dissolved oxygen saturation (at 37 °C and 20 g/kg salinity) = 0.189 mM
Initial concentration of all other metabolites	0 mM
Initial *K. pneumoniae* concentration	0.05 g/L
Initial *B. thetaiotaomicron* concentration	0.0015 g/L
Flow rate (into and out of the reactor)	0.04 L/h
Volumetric oxygen transfer coefficient (Kla)	47.4 h^{-1}
Volume	0.2 L

Table S1.3. The top scoring 50 metabolites involved in the most regulated metabolic pathways, ordered by Z score value. This analysis was performed using gene expression data between samples S8 and S3.

Metabolite name	Number of genes	Number of reactions	Z score
Pyruvate	260	57	1063.96
Phosphoenolpyruvate	174	25	961.45
H+	2468	859	629.11
ADP	964	247	480.86
ATP	1158	326	399.89
H2O	1786	523	350.85
CO2	198	78	306.33
Phosphate	978	259	301.71
D-Glucose	54	9	257.35
Malonyl-[acyl-carrier protein]	50	16	219.07
D-Glucose 6-phosphate	50	13	207.81
H+	726	241	198.26
acyl carrier protein	140	51	195.38
D-Fructose 6-phosphate	46	16	129.56
D-Fructose	26	3	109.83
alpha,alpha-Trehalose 6-phosphate	18	5	105.50
N-Acetyl-D-glucosamine 6-phosphate	20	4	95.97
D-Glucosamine 6-phosphate	18	7	88.31
N-Acetyl-D-glucosamine	22	2	87.79
D-Mannose 6-phosphate	14	5	82.90
N-Acetyl-D-mannosamine 6-phosphate	12	2	81.25
D-Glucose	60	20	77.32
D-Mannose	18	2	75.20
N-Acetyl-D-mannosamine	18	2	75.20
D-Glucosamine	18	2	75.20
Maltose	18	3	73.60
Maltose	22	7	72.65
Glyceraldehyde 3-phosphate	46	14	70.02
Trehalose	20	3	69.47
Acetaldehyde	26	12	67.28

Maltohexaose	26	8	65.21
Maltopentaose	24	7	59.01
Formate	24	5	56.09
Sodium	42	16	54.91
D-Glucose 1-phosphate	30	10	54.58
Maltotetraose	22	6	52.09
N-acetylmuramate 6-phosphate	10	2	48.06
Sodium	50	16	48.02
D-Galactose	22	6	47.82
D-Galactose	20	5	46.58
L-Serine	42	24	45.97
Acetate	42	17	44.94
L-Lactate	8	4	44.93
Glycerol 3-phosphate	42	15	44.41
S-Adenosyl-L-methionine	46	22	43.02
Ubiquinone-8	106	20	41.72
Maltose 6-phosphate	8	1	41.35
S-Adenosyl-L-homocysteine	40	19	41.28
Ubiquinol-8	108	21	39.82
Flavin adenine dinucleotide reduced	28	13	39.73

C h a p t e r 2

RNA Markers Enable Phenotypic Test of Antibiotic Susceptibility in *Neisseria gonorrhoeae* After 10 Minutes of Ciprofloxacin Exposure

Abstract

Antimicrobial-resistant *Neisseria gonorrhoeae* is an urgent public-health threat with continued worldwide incidents of infection and rising resistance to antimicrobials. Traditional culture-based methods for antibiotic susceptibility testing are unacceptably slow (1–2 days), resulting in the use of broad-spectrum antibiotics and the further development and spread of resistance. Critically needed is a rapid antibiotic susceptibility test (AST) that can guide treatment at the point-of-care. Rapid phenotypic approaches using quantification of DNA have been demonstrated for fast-growing organisms (e.g. *E. coli*) but are challenging for slower-growing pathogens such as *N. gonorrhoeae*. Here, we investigate the potential of RNA signatures to provide phenotypic responses to antibiotics in *N. gonorrhoeae* that are faster and greater in magnitude compared with DNA. Using RNA sequencing, we identified antibiotic-responsive transcripts. Significant shifts (>4-fold change) in transcript levels occurred within 5 min of antibiotic exposure. We designed assays for responsive transcripts with the highest abundances and fold changes, and validated gene expression using digital PCR. Using the top two markers (*porB* and *rpmB*) we correctly determined the antibiotic susceptibility and resistance of 49 clinical isolates after 10 min exposure to ciprofloxacin. RNA signatures are therefore promising as an approach on which to build rapid AST devices for *N. gonorrhoeae* at the point-of-care, which is critical for disease management, surveillance, and antibiotic stewardship efforts.

Introduction

Neisseria gonorrhoeae is the second most common sexually transmitted bacterial infection in the United States, with about 460,000 cases reported in 2016, an 18.5% rise since 2015Prevention[1]. Worldwide, it is estimated that about 78 million new *N. gonorrhoeae* infections occur annually[2]. *N. gonorrhoeae* infections can lead to heart and nervous system infections, infertility, ectopic pregnancies, newborn blindness, and increased risk for other sexually transmitted infections, including HIV[3]. The CDC has identified *N. gonorrhoeae* as one of the three most urgent drug-resistant bacterial threats[3]. *N. gonorrhoeae* has developed resistance to all of the most commonly used antibiotics (including penicillins, sulfonamides, tetracyclines, and fluoroquinolones) leaving only one last effective class of antibiotics, cephalosporins. However, there have even been worldwide reported cases of decreased susceptibility to the cephalosporin ceftriaxone[4-8], and therefore an imminent threat of widespread untreatable *N. gonorrhoeae*. An important factor leading to the widespread development of antibiotic resistance is the liberal use and misuse of antibiotics. Critically needed is a rapid antibiotic susceptibility test (AST) that can guide treatment at the point-of-care – both to provide correct treatment and to facilitate antibiotic stewardship.

The gold standard for determining *N. gonorrhoeae* susceptibility to antibiotics is the culture-based agar dilution test, which is unacceptably slow (1–2 days). More rapid genotypic approaches, involving detection of gene mutations, are available for a subset of antibiotics in *N. gonorrhoeae*[9,10], but such approaches are inherently limiting, as they require knowledge of the mechanisms of resistance. Moreover, *N. gonorrhoeae* is naturally competent for transformation, and can take up gonococcal DNA from the environment and recombine it with its own genome, resulting in frequent gene mutations[11,12]. Given the high rate at which new resistance emerges, relying solely on genotypic methods is not an acceptable long-term solution. Phenotypic methods involving growth measurements have enabled faster ASTs that are independent of resistance mechanisms[13-16]. However, such growth-based methods are challenging for *N. gonorrhoeae*, which is slow-growing and fastidious[17]. Another phenotypic approach for antibiotic susceptibility testing is quantification of nucleic acids[18,19]. We have

previously demonstrated a rapid (30 min) phenotypic AST using quantification of DNA replication by digital PCR (dPCR) to assess the antibiotic susceptibility of *Escherichia coli* in clinical urine samples[20]. However, AST methods that quantify changes in DNA replication require a longer antibiotic-exposure step for slow-growing pathogens such as *N. gonorrhoeae,* which has a doubling time of about 60 min[21], compared with the 20 min doubling time of *E. coli*[22].

A complementary approach to DNA quantification is measuring the pathogen's RNA response to antibiotic exposure. Transcriptional responses are among the earliest cellular changes upon exposure to antibiotics[23], far before phenotypic changes in growth can be observed. Quantifying changes in RNA signatures is therefore a particularly appealing approach for slow-growing organisms. RNA has previously been used to differentiate antibiotic susceptibility and resistance in organisms where the transcriptional response is well characterized[24,25]. More recently, RNA sequencing (RNA-Seq) has been used to measure the transcriptome response of *Klebsiella pneumoniae* and *Acinetobacter baumanii* to antibiotic exposure[25]. Although the *N. gonorrhoeae* transcriptome has been previously sequenced[26,27], to our knowledge, no one has characterized the transcriptome response of *N. gonorrhoeae* to antibiotic exposure. Unlike most bacteria, *N. gonorrhoeae* lacks the classic transcriptional SOS response to DNA damage whereby DNA repair is induced and the cell cycle is arrested[28,29]. The SOS response promotes survival to certain antibiotic classes, such as the fluoroquinolones, which act by directly inhibiting DNA synthesis[30]. The recA or recA-like proteins are essential for the induction of the SOS response[28]. However, neither *recA* transcripts nor recA protein levels increase in *N. gonorrhoeae* upon exposure to DNA damaging agents[31,32].

In this work, we explore the transcriptome response of *N. gonorrhoeae* upon exposure to ciprofloxacin. Ciprofloxacin is a fluoroquinolone and functions by inhibiting the enzymes topoisomerase II (DNA gyrase) and topoisomerase IV, thereby inhibiting cell division[33]. Ciprofloxacin was chosen in this study to gain insight into transcriptional changes that occur upon DNA damage in an organism lacking the classic SOS response. Here, we address the

following questions: (1) How does the transcriptome of *N. gonorrhoeae* respond to ciprofloxacin exposure? (2) What is the shortest antibiotic exposure time at which we can still observe significant changes (>4-fold) in RNA expression? (3) Which transcripts provide the largest and most abundant fold-changes per cell, which is an important consideration for clinical samples that have low numbers of pathogens? (4) Will candidate markers respond consistently across a large pool of isolates with wide genetic variability?

Results

We used RNA-seq to study the transcriptome response of susceptible and resistant isolates of *N. gonorrhoeae* after 5, 10, and 15 min of ciprofloxacin exposure (Fig. 2.1). Each clinical isolate was initially split into two tubes, where one tube was exposed to the antibiotic (+) and the other served as the control with no antibiotic exposure (-). Samples were collected for RNA-seq prior to antibiotic exposure and every 5 min for 15 min. We calculated the fold change in gene expression between the control and treated samples – defined as the control:treated ratio (C:T ratio); genes that demonstrated significant fold-change differences between the susceptible and resistant isolates were identified as differentially expressed. To account for biological variability, three pairs of susceptible and resistant isolates were used in this study. Candidate markers were selected from the pool of differentially expressed genes and were validated using droplet dPCR (see Methods).

Temporal shifts in global gene expression upon antibiotic exposure

We observed global shifts in RNA expression in susceptible isolates in as early as 5 min after antibiotic exposure (Fig. 2.2a). The distribution of fold changes in gene expression levels (C:T ratios) indicated global shifts toward negative $\log_2$ fold-change values (downregulation). The magnitude of fold change at which most genes were distributed was approximately 2-fold. The tail of the distribution illustrates that a few genes responded to antibiotic exposure with changes as large as 6-fold within 5 min. Increasing the antibiotic

exposure time further shifted the distribution to larger negative $\log_2$ fold-change values. The transcriptional response in resistant isolates was tightly distributed around a fold-change value of 1 at every time point, indicating that the transcriptome of the resistant isolates did not respond significantly to antibiotic exposure (Fig. 2.2a).

To identify genes that were differentially expressed between control and treated samples, we defined a threshold of significance (Fig. 2.2b). The threshold of significance took into account technical variability and was calculated from the C:T ratios at t = 0 min of all biological replicates that were sequenced (three susceptible and three resistant isolates). For each of the six gene expression datasets (one for each isolate), we plotted the $-\log_2$(C:T ratio) against the $-\log_2$(expression) for all genes and fit a negative exponential curve to the outer edge of each plot. We then averaged the curves from all six datasets and added a 90% confidence interval to the average curve by assuming a Gaussian fit for the error distribution, which we define as our threshold of significance. Genes with a $-\log_2$(C:T ratio) value above or below the upper and lower thresholds were identified as differentially expressed. Downregulated genes (fold changes below the significance threshold) appeared as early as 5 min after antibiotic exposure (blue dots, Fig. 2.2b). Two upregulated genes (fold changes above the significance threshold) appeared after 10 min of exposure (orange dots, Fig. 2.2b).

Selection of candidate markers that are consistent in response and abundant

RNA expression in response to antibiotics can be heterogeneous among different isolates of the same species[34]; thus, it is important to select candidate markers from differentially expressed genes that respond consistently across isolates of *N. gonorrhoeae.* To identify these candidate markers, we exposed three different pairs of susceptible isolates (minimum inhibitory concentrations (MICs) <= 0.015mg/mL) and resistant isolates (MICs 2.0 mg/mL, 4.0mg/mL, and 16.0mg/mL) to ciprofloxacin for 15 min and extracted RNA for sequencing (see workflow in Fig. 2.1). We found 181, 41, and 410 differentially expressed genes in susceptible isolates 1, 2, and 3, respectively (Fig. 2.3a). Among the differentially expressed genes, 38 genes responded consistently across the three pairs of susceptible and resistant isolates (i.e. responses overlapped in all three susceptible isolates, whereas all

three resistant isolates were non-responsive) (Supplementary Table S2.1 online). These genes spanned a variety of biochemical functions in the cell. We selected six candidate transcript markers for further analysis based on the following criteria: (1) high fold change; (2) high expression levels (>75 transcripts per million, TPM); and (3) representative of different biochemical pathways. The selected candidate markers were: *porB* (membrane protein), *rpmB* (ribosomal protein), *tig* (molecular chaperone), *yebC* (transcriptional regulator), *pilB* (pilus assembly ATPase), and *cysK* (cysteine synthase). The candidate marker with the highest abundance and largest fold change upon antibiotic exposure was *porB*, which is a membrane channel forming protein and the site of antibiotic influx into the cell[35].

A high level of gene expression was one of our criteria for selection of candidate markers from the sequencing data. High expression of candidate markers is not only important for sensitivity and limits of detection, but is particularly important for clinical samples with low numbers of pathogen cells. One of the advantages of RNA compared with DNA as a nucleic acid marker is its natural abundance in the cell. Because the gene expression values obtained from sequencing are relative values, our next step was to quantify the absolute copies per cell for the candidate markers. In our quantification approach, we plated clinical isolate samples after 15 min of ciprofloxacin exposure to obtain cell numbers in colony forming units (CFU/mL). We designed primers for the candidate markers (see Methods and Supplementary Table S2) and measured their absolute concentration using dPCR. The concentrations were converted to per cell values using the cell counts from plating (Fig. 2.3b). Additionally, we used the RNA sequencing data to obtain transcriptome-wide estimates of transcript copies per cell. In the sequencing approach, we added external RNA control consortium (ERCC) spike-ins to the lysis buffer step of the extraction protocol in order to capture any loss of RNA throughout the extraction steps. By linear regression, we captured the relationship between ERCC copies added to the samples and ERCC quantified by sequencing. Using the linear regression, we converted gene expression values from RNA sequencing (in TPM) to approximate copy numbers per cell (see Methods). The transcript copies per cell estimated for the candidate markers using the sequencing

approach were within the same order of magnitude as the absolute copies per cell measured by digital PCR (Fig. 2.3b).

Validation of candidate markers by dPCR

We next asked how the relative changes observed through RNA-seq compare with direct gene expression measurements by dPCR. We designed dPCR assays for candidate markers, which involved measuring the absolute expression of the candidate marker in both control and treated samples, and calculating the C:T ratio. In this assay, the 16S rRNA was also measured and used to normalize the C:T ratio of the candidate markers. In the three susceptible isolates that were sequenced we found that rRNA consistently showed the smallest fold change (<1.06) in response to ciprofloxacin compared with all other genes in *N. gonorrhoeae*. Therefore, to account for experimental variations in the antibiotic exposure and RNA extraction steps between control and treated samples, we used the 16S rRNA as an intracellular control for normalizing the C:T ratios (see Methods). We found that the C:T ratios measured by the dPCR assay agreed with the C:T ratios obtained through sequencing (Fig. 2.4), confirming that both approaches accurately capture the transcriptional response to antibiotic exposure.

Validation of RNA markers across CDC isolates

Finally, we asked whether candidate markers respond consistently across a large pool of isolates with genetic variability. We chose the two candidate markers with the highest abundances and fold changes (*porB* and *rpmB*) to determine the susceptibility of 49 clinical isolates, with a wide range of MIC values (Supplementary Table S3 online), from the *N. gonorrhoeae* panel of the Centers for Disease Control (CDC) Antimicrobial Resistance Isolate Bank. The MIC values were representative of the population-wide distribution values reported by the European Committee on Antimicrobial Susceptibility Testing[36]. We exposed each clinical isolate to ciprofloxacin for 10 min and measured the fold change in expression of the two candidate markers between the control and treated sample using dPCR (Fig. 2.5).

Both markers correctly classified all 49 CDC isolates, based on Clinical and Laboratory Standards Institute (CLSI) breakpoint values, as 9 susceptible and 40 resistant strains.

Discussion

In this work, we demonstrate that antibiotic-responsive transcripts can be used as suitable markers for a rapid phenotypic AST in *N. gonorrhoeae.*

When characterizing the global transcriptional response of *N. gonorrhoeae* to antibiotic exposure, we observed a significant change in response in as early as 5 min. The nature of the response was a global downregulation in transcript levels. Among the candidate markers, all exhibited downregulation in response to ciprofloxacin. We specifically looked at *gyrA* and *parC*, which are known genotypic markers of resistance to ciprofloxacin, and differential expression was not observed. We also looked at the *recA* transcript because *recA* is one of the prominent genes in the SOS response, and as expected, because *N. gonorrhoeae* does not have a true SOS system[28,29], we did not find *recA* levels to increase. Whereas *recA* is a specific cellular response to overcome DNA damage, the global downregulation that we observed suggests a general shift away from growth and cell proliferation. Among the 38 candidate markers, 15 were ribosomal proteins (including one of the top markers, *rpmB*), which play a prominent role in assembly and function of the ribosomes and are essential for cell growth. Mutations in ribosomal proteins have been reported to confer resistance to different classes of antibiotics[37]. Another top marker identified in this study was *porB*, which is a membrane channel forming protein (porin) responsible for uptake of small nutrients and the site of antibiotic influx into the cell. The expression of porins is highly regulated in response to environmental stimuli[38]. Reducing permeability to decrease intracellular antibiotic concentration is a known mechanism for bacteria to confer antibiotic resistance[37]. The downregulation of *porB* observed in this study can be attributed to a halt in growth processes caused by ciprofloxacin damage and possibly an attempt to reduce influx of antibiotic.

A key aim of this study was to identify RNA markers that would yield a measurable response after only a short antibiotic exposure (<15 min) to ensure this approach can fit within the required timescale for a rapid AST. It is possible that longer exposure times could provide additional insight into the biological response of *N. gonorrhoeae* to ciprofloxacin, but this was not the focus of our study. Furthermore, the short exposure times potentially introduce a bias in selection of transcripts present at low abundances. For transcripts present at high abundance to display the same fold change as low abundance transcripts, a substantially higher number of mRNA molecules must be transcribed, which would require longer timescales. As an example, a 4-fold change from 1 to 4 transcripts requires 3 additional mRNA to be produced, whereas a 4-fold change from 20 to 80 requires 60 mRNA to be transcribed. This bias also holds true in downregulation, where mRNA continues to be transcribed in the control samples, whereas transcript levels drop in treated samples due to degradation of RNA, and/or a reduction in the rate of transcription.

We identified candidate markers with consistent differential expression across three sets of susceptible and resistant pairs. Among the candidate markers, one of our criteria for selection was transcript abundance, which is of particular importance in clinical samples with low cell numbers. Furthermore, marker abundance affects measurement sensitivity and limits of detection, as has been previously demonstrated in AST methods based on quantification of DNA replication[20]. To measure the abundance of the candidate markers, we used both dPCR measurements and ERCC spike-ins for RNA sequencing to obtain approximate RNA copies/cell. Both methods yielded results within the same order of magnitude. To our knowledge, this is the first quantitative measurement of RNA abundance per cell in *N. gonorrhoeae*.

We separately validated the performance of the two most abundant candidate markers, *porB* and *rpmB*, with 49 clinical isolates. Both markers were consistent in their ability to correctly determine susceptibility or resistance of all 49 clinical isolates. *porB* demonstrated C:T ratios between 2.5 to 7 and *rpmB* demonstrated C:T ratios between 2 and 6 after 10 min of antibiotic exposure in the nine susceptible clinical isolates. The large fold changes highlight the

significance of using RNA response as an AST marker compared with quantification of DNA replication. Our previous work using dPCR quantification of DNA replication demonstrated C:T ratios between 1.2 and 2.4 for 15 min of antibiotic exposure in *E. coli*[20], which has a doubling time approximately 3 times shorter than *N. gonorrhoeae*.

We performed an alignment search of *porB* against other prokaryotes and found it to be specific to the *Neisseria* genus. AST markers should be specific to the pathogen of interest because additional bacterial species are likely to be present in clinical samples. Additional experiments with mixtures of bacteria would be required to further confirm the specificity of the markers identified in this study. We additionally measured the 16s rRNA to normalize C:T ratios, which inherently enables pathogen identification as well. A combination of identification and susceptibility testing in a single integrated platform is important for correct and rapid diagnosis.

This paper demonstrates that RNA markers can be used to determine antibiotic susceptibility of *N. gonorrhoeae* after short antibiotic exposure times, a requirement for a rapid phenotypic AST. *N. gonorrhoeae* is a fastidious slow-growing organism, presenting challenges to growth-based AST methods. Additional work will be needed to yield a clinic-ready, rapid RNA-based AST for *N. gonorrhoeae.* Additional background matrices of clinical samples, both urine and swab samples, that could possibly affect speed and sensitivity of an AST, must be further evaluated. Digital isothermal chemistries, such as digital loop-mediated isothermal amplification (dLAMP) should be considered to speed up quantification times relevant to point-of-care settings[20]. Follow-up studies should also examine the transcriptional response of *N. gonorrhoeae* to other classes of antibiotics and identify responsive RNA markers for class-specific antibiotics. Overall, as a first step, the work described here demonstrates the promise for a phenotypic RNA-based approach for a rapid AST of *N. gonorrhoeae* at the point-of-care, which is critically needed for disease management, surveillance, and antibiotic stewardship.

Methods

Antibiotic exposure for RNA sequencing

Antibiotic susceptible and resistant clinical isolates were obtained from the University of California, Los Angeles, Clinical Microbiology Laboratory. Isolates were plated from glycerol stocks onto Chocolate Agar plates and grown in static incubation overnight (37 °C, 5% CO_2). Cells were re-suspended in Hardy Fastidious Broth (HFB) and incubated for 45 min (37 °C, 5% CO_2) with shaking (800 rpm) to an OD_{600} between 1 and 5. Cultures were diluted (5X) into HFB. Each isolate culture was split into "treated" and "control" tubes. Ciprofloxacin was added to the "treated" tubes (final concentration of 0.5 μg/mL) and water was added to the "control" tubes; cultures were incubated (static; 37 °C, 5% CO_2) for 15 min. During incubation, samples were collected for RNA sequencing at 5, 10, and 15 min (300 μL aliquot of sample was mixed into 600 μL of Qiagen RNA Protect Reagent (Qiagen, Hilden, Germany) for immediate RNA stabilization). In addition, a sample was collected for RNA sequencing immediately before ciprofloxacin was added. To quantify CFU, the sample at t = 15 min was serially diluted (10x), plated on a Chocolate Agar plate, and incubated overnight (37 °C, 5% CO_2).

Antibiotic exposure for clinical isolates

Antibiotic susceptible and resistant clinical isolates were obtained from the *N. gonorrhoeae* panel of the CDC Antimicrobial Resistance Isolate Bank. Isolates were plated from glycerol stocks onto Chocolate Agar plates and grown in static incubation overnight (37 °C, 5% CO_2). Cells were re-suspended in pre-warmed HFB + 5 mM sodium bicarbonate and incubated for 30 min (37 °C, 5% CO_2) with shaking (800 rpm) to an OD_{600} between 1 and 5. Cultures were diluted (100X) into HFB + 5 mM sodium bicarbonate. Each isolate culture was split into treated (0.5 μg/mL final concentration of ciprofloxacin) and control (water instead of antibiotic) samples. Samples were incubated at 37 °C for 10 min on a static hot plate. A 90 μL aliquot of each sample was placed into 180 μL of Qiagen RNA Protect Reagent for immediate RNA stabilization. A 5 μL aliquot of each sample was plated onto a Chocolate

Agar plate and incubated overnight (37 °C, 5% CO_2) as a control for the exposure experiments. If the expected growth phenotypes (i.e. resistant = growth; susceptible = no growth) were not observed for any single sample in the plating control, the exposure experiment was repeated for the set of samples. From the 50 total isolates available from the *N. gonorrhoeae* panel of the CDC Antimicrobial Resistance Isolate Bank, 49 were used in this study. One isolate was excluded from this study because we suspected that it had been contaminated; we did not detect *porB* primer amplification using qPCR.

RNA sequencing and analysis

RNA was extracted using the Enzymatic Lysis of Bacteria protocol of the Qiagen RNeasy Mini Kit and processed according to the manufacturer's protocol. DNA digestion was performed during extraction using the Qiagen RNase-Free DNase Set. The quality of extracted RNA was measured using an Agilent 2200 TapeStation (Agilent, Santa Clara, CA, USA). Extracted RNA samples were prepared for sequencing using the NEBNext Ultra RNA Library Prep Kit for Illumina (New England Biolabs, Ipswitch, MA, USA) and the NEBNExt Multiplex Oligos for Illumina. Libraries were sequenced at 50 single base pair reads and a sequencing depth of 10 million reads on an Illumina HiSeq 2500 System (Illumina, San Diego, CA, USA) at the Millard and Muriel Jacobs Genetics and Genomics Laboratory, California Institute of Technology. Raw reads from the sequenced libraries were subjected to quality control to filter out low-quality reads and trim the adaptor sequences using Trimmomatic (version 0.35). The reads were aligned to the FA 1090 strain of *N. gonorrhoeae* (NCBI Reference Sequence: NC_002946.2) using Bowtie2 (version 2.2.5) and quantified using the Subread package (version 1.5.0-p1). A pseudocount of 1 was added to the gene quantification; gene expression was defined in transcripts per million (TPM).

Marker selection

For each gene, we defined the C:T ratio as the gene expression (TPM) in the control sample divided by the gene expression (in TPM) in the treated sample. We plotted the $-\log_2$(C:T) against the $-\log_2$(expression in TPM) for all genes. To identify genes that were differentially expressed between control and treated samples, we defined a threshold of significance. The threshold of significance was calculated from the C:T ratios at t = 0 min for the biological replicates that were sequenced (three susceptible and three resistant isolates). For each of the six gene expression datasets (one for each isolate), we fit a negative exponential curve to the outer edge of each plot and then averaged the curves from all six datasets. Finally, we added a 90% confidence interval to the average curve by assuming a Gaussian fit for the error distribution, which is our threshold of significance. Genes with a $-\log_2$(C:T) value above or below the upper and lower thresholds were identified as differentially expressed. Genes that were differentially expressed consistently (either always above or always below the thresholds) among the three susceptible isolates and were not differentially expressed among the three resistant isolates were defined as candidate markers.

Copies/cell measurements from sequencing

To measure copies per cell using sequencing data, we added 2uL of (1/1000 dilution) ERCC RNA Spike-In Mix (Thermo Fisher Scientific, Waltham, MA, USA) to the lysis buffer in the RNeasy Mini Kit to each individual sample. We calculated the number of copies of each ERCC transcript in the sample, by accounting for dilution and multiplying by Avogadro's number (manufacturer's concentrations were reported in attomoles/μL). We plotted the relationship between $\log_2$(ERCC copies added) against $\log_2$(gene expression in TPM) and performed a linear regression in the region of linearity. We used the linear regression to convert TPM values to total RNA copies in each sample. Finally, using the CFU measured for each sample from plating (described in the "Antibiotic exposure for RNA sequencing" section), the total RNA copies were converted to copies per cell.

Validation with droplet digital PCR (dPCR)

Primers were designed for candidate markers using Primer-BLAST[39] and primer alignments were verified using SnapGene. Expression of candidate markers was quantified using the Bio-Rad QX200 droplet dPCR system (Bio-Rad Laboratories, Hercules, CA, USA). The concentration of the components in the dPCR mix used in this study were as follows: 1× EvaGreen Droplet Generation Mix (Bio-Rad), 150U/mL WarmStart RTx Reverse Transcriptase, 800U/mL RiboGaurd RNase Inhibitor, 500 nM forward primer, and 500 nM reverse primer. The RNA extraction comprised 5% of the final volume in the dPCR mix. The remaining volume was nuclease-free water. For each isolate, candidate marker expression was quantified in the control and treated samples and the fold-change difference (C:T ratio) was calculated. To account for potential differences between the control and treated samples that could arise from experimental variability and extraction efficiency, we used ribosomal RNA (rRNA) as an internal control because from our sequencing data, we found that rRNA was not affected by antibiotic exposure in the time frame of this study. To normalize by rRNA, we quantified the 16S rRNA in the control and treated samples by dPCR and calculated an rRNA C:T ratio. We then divided the C:T ratio of each marker by the rRNA C:T ratio. All dPCR C:T ratios reported in this paper are the normalized C:T ratios.

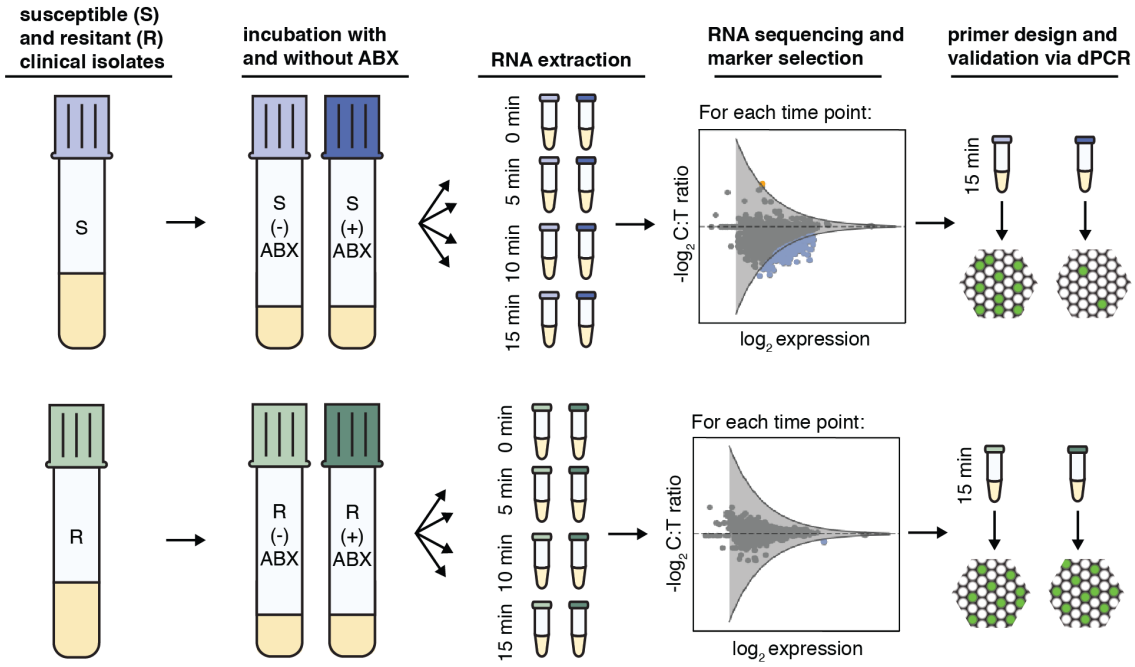

Figure 2.1. The workflow for selection and validation of RNA markers for phenotypic measurements of antibiotic susceptibility and resistance. Susceptible and resistant isolates of *Neisseria gonorrhoeae* are exposed to antibiotics (ABX) for 5, 10, and 15 min. Samples are collected for RNA sequencing at time zero and every 5 min thereafter. Genes demonstrating fold changes in expression (control:treated ratio (C:T ratio)) greater than the threshold of significance (gray line) are identified as differentially expressed (blue: downregulated and orange: upregulated). Candidate markers are selected from the pool of differentially expressed genes and validated by digital PCR.

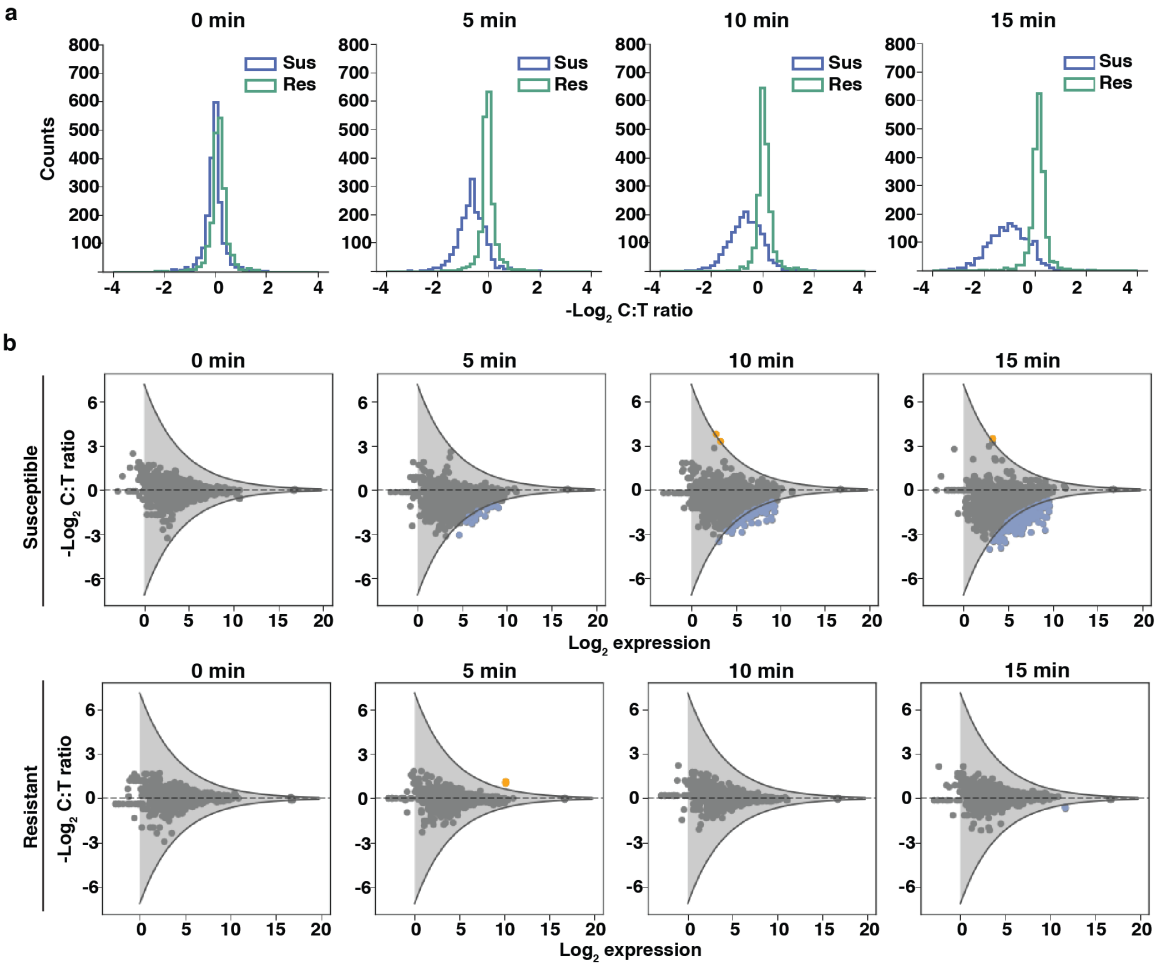

Figure 2.2. Temporal shifts in global gene expression upon ciprofloxacin exposure in *Neisseria gonorrhoeae*. (**a**) The distribution of -log$_2$(C:T ratios) for a susceptible isolate (Sus) and resistant isolate (Res) at 0, 5, 10, and 15 min. (**b**) The fold change in gene expression between control and treated samples (C:T ratio) versus expression in the control sample at 0, 5, 10, and 15 min for one susceptible isolate and one resistant isolate. Genes with C:T ratios above or below the significance threshold are identified as differentially expressed (blue: downregulated; orange: upregulated). Thresholds for statistical significance of fold change (gray lines) are determined by fitting a negative exponential curve (with 90% confidence interval) to the outer edge of the -log$_2$ C:T ratios measured at time zero (see Methods).

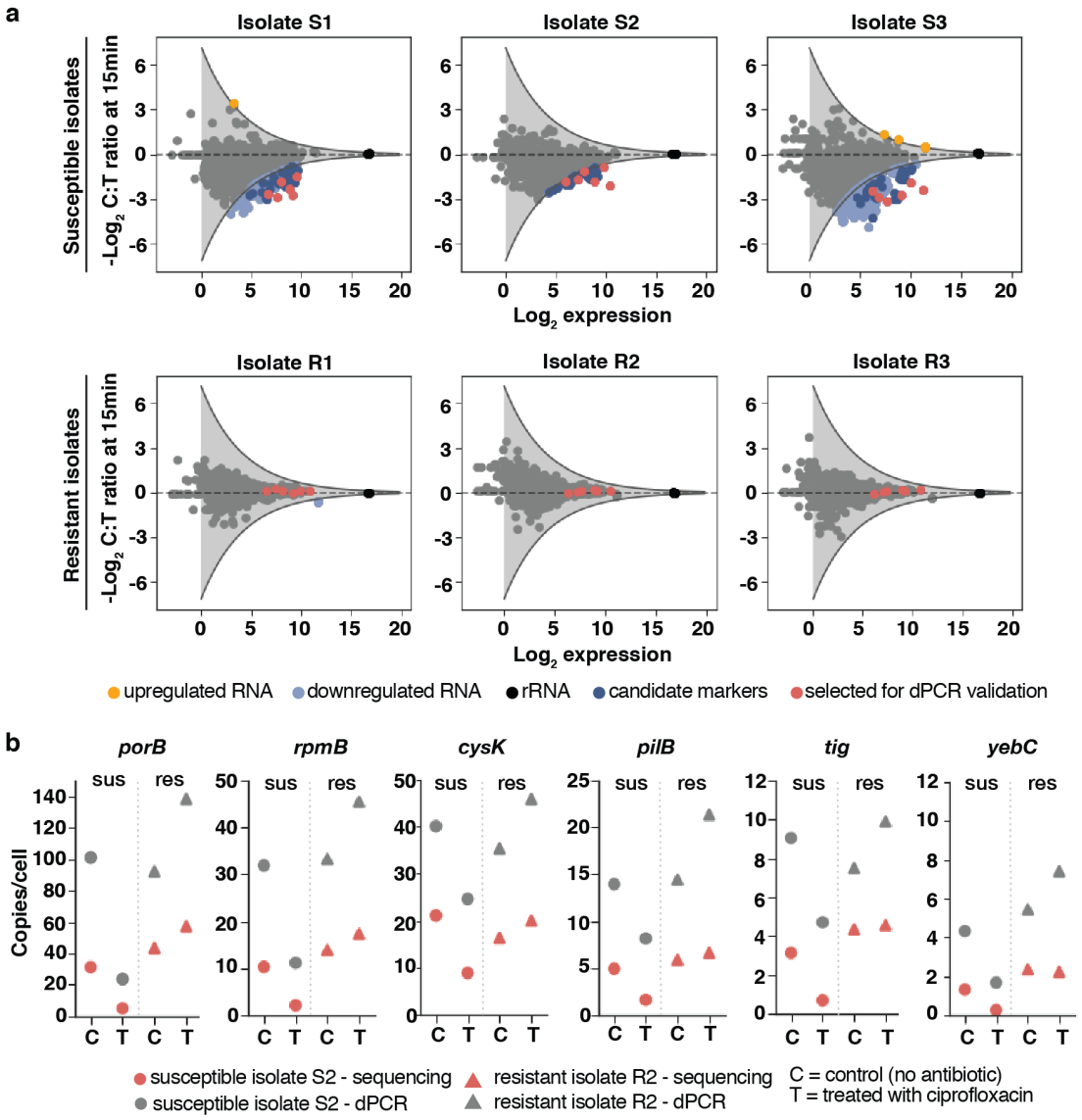

Figure 2.3. Selection of candidate RNA markers for phenotypic antibiotic susceptibility testing in *Neisseria gonorrhoeae* and measurements of candidate marker abundances per cell (**a**) Genes that are differentially expressed (light blue) across three pairs of resistant and susceptible clinical isolates are identified as candidate markers (dark blue). Six candidate markers that span different biological functions were selected for validation (red). (**b**) Copies/cell values for the candidate markers are determined from RNA sequencing (red) and dPCR (gray) (see Methods). Data is shown for one pair of susceptible (S2) and resistant (R2) isolates at 15 min of ciprofloxacin exposure.

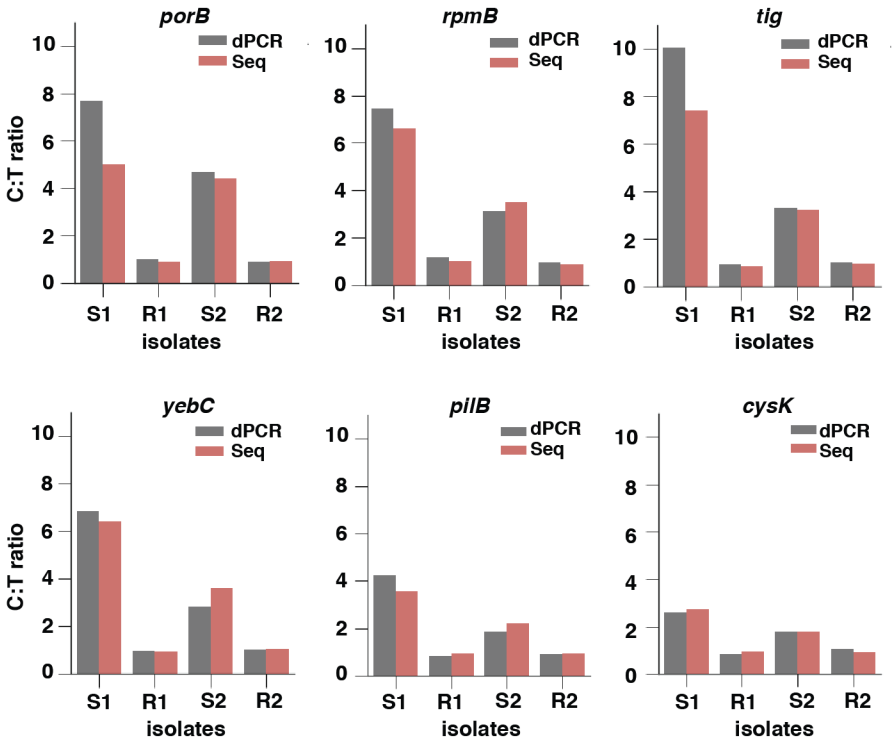

Figure 2.4. Validation of the RNA sequencing approach using digital PCR (dPCR) with six candidate markers. Control:treated ratios (C:T ratios) determined by RNA sequencing (red) were validated against C:T ratios measured by dPCR (gray). The dPCR C:T ratios were normalized using ribosomal RNA (rRNA) by dividing the C:T ratio of the candidate marker by the C:T ratio of 16S rRNA. This normalization step is not required for sequencing data because sequencing depth normalizes the values (see Methods). Markers were validated using two susceptible (S1 and S2) and two resistant (R1 and R2) isolates at 15 min of ciprofloxacin exposure.

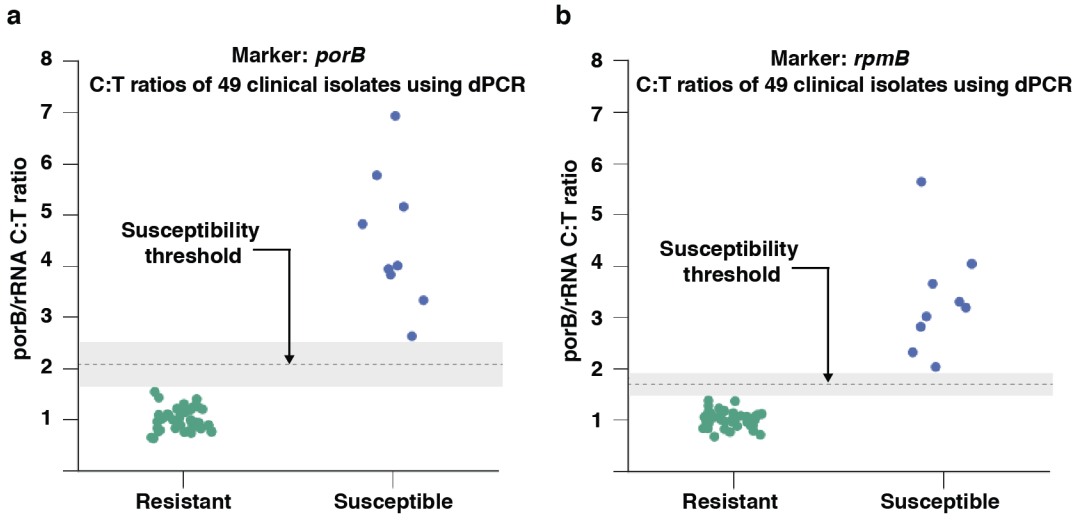

Figure 2.5. Antibiotic susceptibility testing of 49 clinical isolates using (a) *porB* and (b) *rpmB* as RNA AST markers. Antibiotic susceptibility of 49 clinical isolates (9 susceptible and 40 resistant) from the *Neisseria gonorrhoeae* panel of the CDC bacteria bank was determined using the "normalized" C:T ratios (C:T ratio of marker/C:T ratio of 16S rRNA). Clinical isolates were exposed to ciprofloxacin for 10 min and the concentration of RNA markers was measured by digital PCR.

References

1 Centers for Disease Control and Prevention. Sexually transmitted disease surveillance, 2016 (2017).

2 World Health Organization. Global action plan to control the spread and impact of antimicrobial resistance in *Neisseria gonorrhoeae* (2012).

3 Centers for Disease Control and Prevention. Antibiotic resistance threats in the United States, 2013 (2013).

4 Unemo, M. *et al.* High-level cefixime-and ceftriaxone-resistant *Neisseria gonorrhoeae* in France: novel penA mosaic allele in a successful international clone causes treatment failure. *Antimicrob. Agents Chemother.* **56**, 1273-1280 (2012).

5 Ohnishi, M. *et al.* ceftriaxone-resistant *Neisseria gonorrhoeae*, Japan. *Emerg. Infect. Dis.* **17**, 148 (2011).

6 Lahra, M. M., Ryder, N. & Whiley, D. M. A new multidrug-resistant strain of *Neisseria gonorrhoeae* in Australia. *N. Engl. J. Med.* **371**, 1850-1851 (2014).

7 Cámara, J. *et al.* Molecular characterization of two high-level ceftriaxone-resistant *Neisseria gonorrhoeae* isolates detected in Catalonia, Spain. *J. Antimicrob. Chemother.* **67**, 1858-1860 (2012).

8 Deguchi, T. *et al.* New clinical strain of *Neisseria gonorrhoeae* with decreased susceptibility to ceftriaxone, Japan. *Emerg. Infect. Dis.* **22**, 142 (2016).

9 Hemarajata, P., Yang, S., Soge, O., Humphries, R. & Klausner, J. Performance and verification of a real-time PCR assay targeting the gyrA gene for prediction of ciprofloxacin resistance in *Neisseria gonorrhoeae*. *J. Clin. Microbiol.* **54**, 805-808 (2016).

10 Pond, M. J. *et al.* Accurate detection of *Neisseria gonorrhoeae* ciprofloxacin susceptibility directly from genital and extragenital clinical samples: towards genotype-guided antimicrobial therapy. *J. Antimicrob. Chemother.* **71**, 897-902 (2016).

11 Aas, F. E., Løvold, C. & Koomey, M. An inhibitor of DNA binding and uptake events dictates the proficiency of genetic transformation in *Neisseria gonorrhoeae*:

mechanism of action and links to type IV pilus expression. *Mol. Microbiol.* **46**, 1441-1450 (2002).

12 Hamilton, H. L. & Dillard, J. P. Natural transformation of *Neisseria gonorrhoeae*: from DNA donation to homologous recombination. *Mol. Microbiol.* **59**, 376-385 (2006).

13 Baltekin, Ö., Boucharin, A., Tano, E., Andersson, D. I. & Elf, J. Antibiotic susceptibility testing in less than 30 min using direct single-cell imaging. *Proc. Natl. Acad. Sci. U.S.A.*, 201708558 (2017).

14 Liu, T.-T. *et al.* A high speed detection platform based on surface-enhanced Raman scattering for monitoring antibiotic-induced chemical changes in bacteria cell wall. *PloS One* **4**, e5470 (2009).

15 Broeren, M., Maas, Y., Retera, E. & Arents, N. Antimicrobial susceptibility testing in 90 min by bacterial cell count monitoring. *Clin. Microbiol. Infect.* **19**, 286-291 (2013).

16 Fredborg, M. *et al.* Real-time optical antimicrobial susceptibility testing. *J. Clin. Microbiol.* **51**, 2047-2053 (2013).

17 Spence, J. M., Wright, L. & Clark, V. L. Laboratory maintenance of *Neisseria gonorrhoeae*. *Curr. Protoc. Microbiol.*, 4A. 1.1-4A. 1.26 (2008).

18 Mezger, A. *et al.* A general method for rapid determination of antibiotic susceptibility and species in bacterial infections. *J. Clin. Microbiol.* **53**, 425-432 (2015).

19 Rolain, J., Mallet, M., Fournier, P. & Raoult, D. Real-time PCR for universal antibiotic susceptibility testing. *J. Antimicrob. Chemother.* **54**, 538-541 (2004).

20 Schoepp, N. G. *et al.* Rapid pathogen-specific phenotypic antibiotic susceptibility testing using digital LAMP quantification in clinical samples. *Sci. Transl. Med.* **9**, eaal3693 (2017).

21 Tobiason, D. M. & Seifert, H. S. The obligate human pathogen, *Neisseria gonorrhoeae*, is polyploid. *PLoS Biol.* **4**, e185 (2006).

22 Cooper, S. & Helmstetter, C. E. Chromosome replication and the division cycle of *Escherichia coli* Br. *J. Mol. Biol.* **31**, 519-540 (1968).

23 Sangurdekar, D. P., Srienc, F. & Khodursky, A. B. A classification based framework for quantitative description of large-scale microarray data. *Genome Biol.* **7**, R32 (2006).

24 Barczak, A. K. *et al.* RNA signatures allow rapid identification of pathogens and antibiotic susceptibilities. *Proc. Natl. Acad. Sci. U.S.A.* **109**, 6217-6222 (2012).

25 Bhattacharyya, R. *et al.* Rapid Phenotypic Antibiotic Susceptibility Testing Through RNA Detection. *Open Forum Infect. Dis.* **4**, S33-S33, 10.1093/ofid/ofx162.082 (2017).

26 McClure, R. *et al.* The gonococcal transcriptome during infection of the lower genital tract in women. *PloS One* **10**, e0133982 (2015).

27 Remmele, C. W. *et al.* Transcriptional landscape and essential genes of Neisseria gonorrhoeae. *Nucleic Acids Res.* **42**, 10579-10595 (2014).

28 Stohl, E. A., Gruenig, M. C., Cox, M. M. & Seifert, H. S. Purification and characterization of the RecA protein from *Neisseria gonorrhoeae*. *PloS One* **6**, e17101 (2011).

29 Schook, P. O., Stohl, E. A., Criss, A. K. & Seifert, H. S. The DNA-binding activity of the Neisseria gonorrhoeae LexA orthologue NG1427 is modulated by oxidation. *Mol. Microbiol.* **79**, 846-860 (2011).

30 Qin, T.-T. *et al.* SOS response and its regulation on the fluoroquinolone resistance. *Ann. Transl. Med.* **3** (2015).

31 Black, C. G., Fyfe, J. A. & Davies, J. K. Absence of an SOS-like system in *Neisseria gonorrhoeae*. *Gene* **208**, 61-66 (1998).

32 Stohl, E. A. & Seifert, H. S. *Neisseria gonorrhoeae* DNA recombination and repair enzymes protect against oxidative damage caused by hydrogen peroxide. *J. Bacteriol.* **188**, 7645-7651 (2006).

33 LeBel, M. Ciprofloxacin: chemistry, mechanism of action, resistance, antimicrobial spectrum, pharmacokinetics, clinical trials, and adverse reactions. *Pharmacotherapy* **8**, 3-30 (1988).

34 Gao, Q. *et al.* Gene expression diversity among *Mycobacterium tuberculosis* clinical isolates. *Microbiology* **151**, 5-14 (2005).

35 Quillin, S. J. & Seifert, H. S. *Neisseria gonorrhoeae* host adaptation and pathogenesis. *Nat. Rev. Microbiol.* **16**, 226-240 (2018).

36 The European Committee on Antimicrobial Susceptibility Testing. Ciprofloxacin/*Neisseria gonorrhoeae* International MIC Distribution - Reference Database 2018-04-03. https://mic.eucast.org/Eucast2/regShow.jsp?Id=35702 (2018).

37 Gomez, J. E. *et al.* Ribosomal mutations promote the evolution of antibiotic resistance in a multidrug environment. *Elife* **6** (2017).

38 Fernández, L. & Hancock, R. E. Adaptive and mutational resistance: role of porins and efflux pumps in drug resistance. *Clin. Microbiol. Rev.* **25**, 661-681 (2012).

39 Ye, J. *et al.* Primer-BLAST: a tool to design target-specific primers for polymerase chain reaction. *BMC Bioinformatics* **13**, 134 (2012).

Supplementary Information

Supplementary Table S2.1. List of candidate markers and their expression in transcripts per million (TPM) and copies per cell for susceptible isolate S2 and resistant isolate R2 after 15 min of ciprofloxacin exposure. The genome used for alignment was *N. gonorrhoeae* FA1090 (NCBI Reference Sequence: NC_002946.2).

		Susceptible (S2) Control		Susceptible (S2) Treated		Resistant (R2) Control		Resistant (R2) Treated	
Locus Tag	**Gene Description**	**TPM**	**copies/cell**	**TPM**	**copies/cell**	**TPM**	**copies/cell**	**TPM**	**copies/cell**
NGO0340	cysteine synthase A (*cysK*)	894.1	21.1	505.2	8.9	551.8	16.3	600.0	20.0
NGO1837	50S ribosomal protein L4 *(rplD*)	474.9	10.8	262.2	4.4	403.6	11.9	425.4	13.8
NGO1843	elongation factor G (fusA)	433.4	9.8	224.9	3.8	432.9	12.8	503.5	16.6
NGO2024	50S ribosomal protein L13 (*rplM*)	415.0	9.4	213.5	3.6	455.3	13.5	503.5	16.6
NGO1845	30S ribosomal protein S12 (*rpsL*)	563.1	13.0	286.8	4.9	615.4	18.2	697.6	23.5
NGO1677	50S ribosomal protein L27 (rpmA)	410.7	9.3	192.2	3.2	500.6	14.8	497.6	16.4
NGO1844	30S ribosomal protein S7	520.0	11.9	241.3	4.0	520.1	15.4	651.6	21.9
NGO0171	50S ribosomal protein L19 (*rplS*)	379.2	8.5	175.0	2.9	328.5	9.7	353.2	11.3
NGO1834	30S ribosomal protein S19 (*rpsS*)	330.0	7.4	152.1	2.5	260.9	7.7	292.7	9.2
NGO0172	tRNA (guanine-N(1)-)-methyltransferase (*trmD*)	237.3	5.2	108.8	1.7	208.8	6.2	224.6	6.9
NGO1835	50S ribosomal protein L2 (*rplB*)	392.5	8.9	179.1	2.9	297.6	8.8	359.8	11.5
NGO1673	type IV pilus assembly protein (*pilB*)	225.9	4.9	101.5	1.6	199.3	5.9	214.9	6.6
NGO1833	50S ribosomal protein L22 (*rplV*)	343.8	7.7	147.9	2.4	292.1	8.6	304.3	9.6
NGO2173	50S ribosomal protein L32 (*rpmF*)	407.5	9.2	173.6	2.9	394.7	11.7	404.1	13.1
NGO0604	30S ribosomal protein S1 (*rpsA*)	437.9	9.9	185.3	3.1	456.3	13.5	493.9	16.2
NGO0016	preprotein translocase subunit (*secG*)	180.1	3.9	73.7	1.1	169.1	5.0	184.5	5.6
NGO2174	hypothetical protein	372.8	8.4	150.2	2.4	368.3	10.9	361.6	11.6
NGO2164	GMP synthase (guaA)	118.3	2.5	45.0	0.7	98.6	2.9	109.4	3.2
NGO1676	50S ribosomal protein L21 (*rplU*)	554.6	12.8	200.4	3.3	555.2	16.4	587.7	19.6

NGO1679	50S ribosomal protein L33 (*rpmG*)	283.8	6.3	101.4	1.6	298.5	8.8	284.3	8.9
NGO1658	hypothetical protein	98.4	2.1	33.8	0.5	118.3	3.5	116.1	3.4
NGO1440	macrolide transport protein MacA	143.3	3.1	48.6	0.7	132.3	3.9	139.7	4.2
NGO0174	30S ribosomal protein S16 (*rpsP*)	315.2	7.0	101.2	1.6	295.8	8.7	340.5	10.9
NGO0173	ribosome maturation factor RimM (*rimM*)	359.8	8.1	113.5	1.8	316.8	9.4	318.8	10.1
NGO0592	trigger factor (*tig*)	146.5	3.1	45.5	0.7	147.5	4.3	152.1	4.6
NGO1680	50S ribosomal protein L28 (*rpmB*)	452.8	10.3	130.3	2.1	470.2	13.9	525.4	17.3
NGO0620	aspartate alpha-decarboxylase	64.8	1.3	18.6	0.3	54.2	1.6	59.3	1.7
NGO1659	intracellular septation protein A	62.2	1.3	17.8	0.3	63.6	1.9	70.7	2.0
NGO1291	transcriptional regulator (yebC)	64.1	1.3	18.0	0.3	79.9	2.3	77.9	2.2
NGO0648	membrane protein	56.4	1.1	15.3	0.2	47.6	1.4	45.2	1.2
NGO0593	ATP-dependent Clp protease proteolytic subunit (*clpP*)	60.2	1.2	16.0	0.2	73.6	2.2	75.9	2.2
NGO1804	(3R)-hydroxymyristoyl-ACP dehydratase (*fabZ*)	91.0	1.9	24.0	0.3	74.6	2.2	73.5	2.1
NGO0618	membrane protein	81.4	1.7	20.1	0.3	66.8	2.0	70.2	2.0
NGO0619	2-dehydro-3-deoxyphosphooctonate aldolase	61.1	1.2	15.1	0.2	51.1	1.5	62.6	1.8
NGO1812	major outer membrane protein (*porB*)	1293.2	31.2	293.4	5.0	1459.1	43.3	1587.1	57.1
NGO1890	glutamate permease; sodium/glutamate symport carrier protein	35.0	0.7	7.5	0.1	40.3	1.2	48.9	1.3
NGO2098	diaminopimelate decarboxylase	26.0	0.5	4.9	0.1	18.6	0.5	18.6	0.5
NGO2100	frataxin-like protein (*cyaY*)	20.4	0.4	3.6	0.0	14.0	0.4	18.1	0.5

Supplementary Table S2.2. Primer sequences used for validation of candidate markers by digital PCR.

Candidate Marker	Gene Name	Forward Primer Sequence	Reverse Primer Sequence
porB	major outer membrane porin	GCTACGATTCTCCCGAATTTGCC	CCGCCKACCAAACGGTGAAC
rpmB	50S ribosomal protein L28	TTGCCCAACTTGCAATCACG	AGCACGCAAATCAGCCAATAC
tig	trigger factor	AAAGCCTTGGGTATTGCGG	TGACCAAAGCAACCGGAAC
yebC	YebC/PmpR family Transcriptional Regulator	GCTTTGGAAAAAGCAGCCG	GGTTTTGTTGTCGGTCAGGC
pilB	Type IV-A pilus assembly ATPase	GACTTTTGCCGCTGCTTTG	GCGCATTATTCGTGTGCAG
cysK	Cysteine synthase A	GAGGCTTCCCCCGTATTGAG	TTCAAAAGCCGCTTCGTTCG
16S rRNA	16S ribosomal RNA	ACTGCGTTCTGAACTGGGTG	GGCGGTCAATTTCACGCG

Supplementary Table S2.3. Minimum inhibitory concentration **(**MIC) values for the 49 *Neisseria gonorrhoeae* clinical isolates acquired from the CDC and FDA Antibiotic Resistance Isolate Bank[1].

MIC	Number of strains	Susceptible or Resistant
0.015	8	Susceptible
0.03	1	Susceptible
4	1	Resistant
8	6	Resistant
16	33	Resistant

[1] CDC and FDA Antibiotic Resistance Isolate Bank. Atlanta (GA): CDC. (2018)